Commun. Comput. Phys.
doi: 10.4208/cicp.2009.08.181

Vol. 7, No. 1, pp. 64-102
January 2010

The Riemann Problem for the Dispersive Nonlinear Shallow Water Equations

Giovanna Grosso[1,*], Matteo Antuono[2] and Eleuterio Toro[3]

[1] *DICAT, University of Genova, Via Montallegro 1, I-16145 Genova, Italy.*
[2] *INSEAN (The Italian Ship Model Basin), Via di Vallerano 139, 00128, Roma, Italy.*
[3] *Laboratory of Applied Mathematics, University of Trento, Via Mesiano 77, I-38100 Trento, Italy.*

Received 24 November 2008; Accepted (in revised version) 30 March 2009

Communicated by Chi-Wang Shu

Available online 16 July 2009

Abstract. The complete analytical solution of the Riemann problem for the homogeneous Dispersive Nonlinear Shallow Water Equations [Antuono, Liapidevskii and Brocchini, Stud. Appl. Math., 122 (2009), pp. 1-28] is presented, for both wet-bed and dry-bed conditions. Moreover, such a set of hyperbolic and dispersive depth-averaged equations shows an interesting resonance phenomenon in the wave pattern of the solution and we define conditions for the occurrence of resonance and present an algorithm to capture it. As an indirect check on the analytical solution we have carried out a detailed comparison with the numerical solution of the government equations obtained from a dissipative method that does not make explicit use of the solution of the local Riemann problem.

PACS: 47.11.-j, 02.70.-c, 47.35.-i

Key words: Riemann problem, Dispersive Nonlinear Shallow Water Equations, compound waves, resonance.

1 Introduction: The Dispersive Nonlinear Shallow Water Equations

The most popular approximate model equations for studying nearshore hydrodynamics are the Nonlinear Shallow Water Equations (NSWE) and many available Boussinesq type equations (BTEs), which all stem from the work of Peregrine [12]. BTEs are capable to model dispersive effects and are valid throughout a wide portion of the nearshore

*Corresponding author. *Email addresses:* ggrosso@dicat.unige.it (G. Grosso), m.antuono@insean.it (M. Antuono), toro@ing.unitn.it (E. Toro)

zone, but they cannot directly account for wave breaking and they cannot intrinsically predict the motion or the position of the shoreline [3]. On the contrary, the classical Nonlinear Shallow Water Equations allow for a simple treatment of wave breaking and of the shoreline motion, but they cannot model dispersive effects and their validity is limited to a narrow area close to the shore. In order to combine the advantages of these models, Antuono, Liapidevskii and Brocchini [1] proposed a new set of depth-averaged equations, called Dispersive Nonlinear Shallow Water Equations (DNSWE), which are dispersive and hyperbolic at the same time. These equations, obtained by using a hyperbolic approximation of a chosen set of nonlinear and weakly-dispersive Boussinesq-type equations, provide both a physically sound description of the nearshore dynamics and a complete representation of dispersive and nonlinear wave phenomena. A detailed description of the conditioning of the dispersive terms and of the related hyperbolic approximation can be found in Antuono, Liapidevskii & Brocchini [1]. Here, a complete description of the main advantages of the DNSWE is also given.

The 1D set of dimensional DNSWE can be written in the following conservative form:

$$\begin{cases} d_t + Q_x = 0, \\ \left[Q\left(1 - \dfrac{h_{xx}}{6} d\right) \right]_t + \left(\dfrac{g d^2}{2} + \dfrac{Q^2}{d} + \dfrac{A d^2}{3} \psi - \dfrac{g h_x^2}{6} d^2 \right)_x \\ \quad = \dfrac{A h_x}{3} d\psi - g \dfrac{h_x^3}{3} d - g \dfrac{h_x h_{xx}}{3} d^2 + g h_x d, \\ \phi_t = \psi, \\ \gamma \psi_t + Q_x = -A\phi, \end{cases} \tag{1.1}$$

where $Q = ud$ is the flow rate, A is a positive dimensional parameter ($[A] = T^{-2}$) generally set to $1 s^{-2}$, γ is a positive dimensionless parameter ($\gamma \ll 1$) and ϕ and ψ are two potential functions. As shown in Fig. 1, h is the still water level, u is the onshore velocity and d is the total water depth.

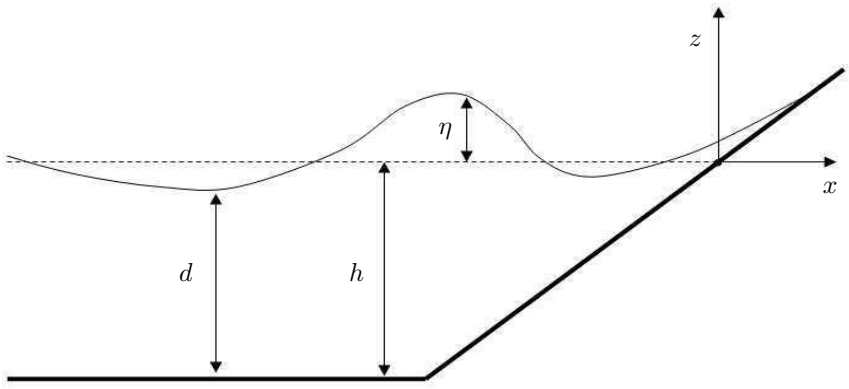

Figure 1: The reference frame of the DNSWE.

In the case of smooth bathymetries, i.e. assuming $h_{xx} \ll 1$ and $h_x^2/3 \ll 1$, we get

$$\begin{cases} d_t + Q_x = 0, \\ Q_t + \left(\dfrac{gd^2}{2} + \dfrac{Q^2}{d} + \dfrac{Ad^2}{3}\psi \right)_x = h_x d \left(g + \dfrac{A\psi}{3} \right), \\ \phi_t = \psi, \\ \psi_t + \dfrac{Q_x}{\gamma} = -\dfrac{A}{\gamma}\phi. \end{cases} \tag{1.2}$$

The hyperbolic system of balance laws (1.2) can be written as follows:

$$\frac{\partial}{\partial t}\mathbf{U} + \frac{\partial}{\partial x}\mathbf{F}(\mathbf{U}) = \mathbf{S}(\mathbf{U}). \tag{1.3}$$

Then, the homogeneous system associated to (1.3) is:

$$\frac{\partial}{\partial t}\mathbf{U} + \frac{\partial}{\partial x}\mathbf{F}(\mathbf{U}) = \mathbf{0}, \tag{1.4}$$

which is a hyperbolic system of conservation laws, while the divergence free system associated to (1.3) is:

$$\frac{\partial}{\partial t}\mathbf{U} = \mathbf{S}(\mathbf{U}), \tag{1.5}$$

which is a system of ordinary differential equations. Two processes are involved in the system of balance laws (1.3): a conservative process associated to the homogeneous part (1.4) with a characteristic speed v_f and a dissipative/productive process associated to the divergence-free part (1.5) with a characteristic speed v_s. Because of the presence of the small parameter γ, the ratio $\epsilon = v_f/v_s$ is very small ($\epsilon \ll 1$); hence the dissipative/productive process is much faster than the conservative one and the source term is said to be stiff.

In order to solve systems of balance laws with stiff source terms, splitting schemes are very commonly used (see [2, 5, 6, 10]). These schemes consist in iteratively solving the associated system of conservation laws with a classical finite volume scheme and the associated system of ordinary differential equations with an appropriate numerical tool. In particular, powerful numerical fluxes to solve hyperbolic systems of conservation laws, like (1.4), are based on the solution of the Riemann problem for the system of conservation laws, for example the fluxes of Godunov [7], Osher [4, 11] and Roe [14] (for a review see [16]). Hence, the aim of the present work is to propose the exact solution of the Riemann problem for the homogeneous part of the DNSWE (1.2). In Section 2 the eigenstructure of the homogeneous DNSWE is studied, in Section 3 the canonical wave structure of the solution of the Riemann problem is shown, while in Section 4 the resonance phenomenon is analyzed in depth to obtain the related wave configuration. In Sections 5 and 6 a solution strategy is proposed, while in Section 7 the dry-bed Riemann problem is studied in detail. Section 8 presents a comparison of the proposed analytical solution with numerical solutions of the problem. In Section 9, a summary with conclusions and future research goals is given.

2 The Riemann problem for the homogeneous DNSWE

The Riemann problem for the homogeneous part of system (1.2) is defined as the initial-value problem

$$\left.\begin{array}{l} \text{PDEs}: \mathbf{U}_t + \mathbf{F}(\mathbf{U})_x = \mathbf{0}, \\ \text{ICs}: \mathbf{U}(x,0) = \left\{ \begin{array}{ll} \mathbf{U}_L & \text{if} \quad x<0, \\ \mathbf{U}_R & \text{if} \quad x>0, \end{array} \right. \end{array}\right\} \tag{2.1}$$

where $\mathbf{U}$ and $\mathbf{F}$ are the vector of the unknowns and the flux vector

$$\mathbf{U} = \begin{bmatrix} d \\ Q \\ \phi \\ \psi \end{bmatrix}, \qquad \mathbf{F} = \begin{bmatrix} Q \\ \dfrac{gd^2}{2} + \dfrac{Q^2}{d} + \dfrac{Ad^2}{3}\psi \\ 0 \\ \dfrac{Q}{\gamma} \end{bmatrix}, \tag{2.2}$$

and the initial states $\mathbf{U}_L$ and $\mathbf{U}_R$

$$\mathbf{U}_L = \begin{bmatrix} d_L \\ Q_L \\ \phi_L \\ \psi_L \end{bmatrix}, \qquad \mathbf{U}_R = \begin{bmatrix} d_R \\ Q_R \\ \phi_R \\ \psi_R \end{bmatrix} \tag{2.3}$$

are constant vectors and represent conditions at time $t=0$ to the left of $x=0$ and to the right of $x=0$, respectively. Although the third equation of the system gives the trivial solution $\phi = const.$, we still keep it, as its contribution is not negligible when coupled to the respective equation of system (1.5).

2.1 Eigenvalues and Eigenvectors

In order to solve the Riemann problem (2.1), it is necessary to study the eigenstructure of the equations, i.e. compute the eigenvalues and eigenvectors of the system (1.4). In fact, these quantities allow to understand the mathematical character of the governing equations and the physical character of free-surface waves. For more details on the hyperbolic theory see [15, 16].

Let us write equations (1.4) in the form:

$$\partial_t \mathbf{U} + \mathbf{A}\partial_x \mathbf{U} = 0, \tag{2.4}$$

where $\mathbf{A}$ is the jacobian matrix of $\mathbf{F}$, i.e. $A_{ij} = \frac{\partial F_i}{\partial U_j}$

$$\mathbf{A} = \begin{bmatrix} 0 & 1 & 0 & 0 \\ gd - \dfrac{Q^2}{d^2} + \dfrac{2}{3}ad\psi & \dfrac{2Q}{d} & 0 & \dfrac{ad^2}{3} \\ 0 & 0 & 0 & 0 \\ 0 & \dfrac{1}{\gamma} & 0 & 0 \end{bmatrix}. \tag{2.5}$$

The eigenvalues of **A** are:

$$\lambda_1 = \frac{Q}{d} - \sqrt{gd + \frac{Ad^2}{3\gamma} + \frac{2}{3}Ad\psi}, \tag{2.6a}$$

$$\lambda_2 = 0, \tag{2.6b}$$

$$\lambda_3 = 0, \tag{2.6c}$$

$$\lambda_4 = \frac{Q}{d} + \sqrt{gd + \frac{Ad^2}{3\gamma} + \frac{2}{3}Ad\psi}, \tag{2.6d}$$

while the right eigenvectors associated to the previous eigenvalues are:

$$\mathbf{R}^{(1)} = \begin{bmatrix} \gamma \\ \gamma\left[\frac{Q}{d} - \sqrt{gd + \frac{Ad^2}{3\gamma} + \frac{2}{3}Ad\psi}\right] \\ 0 \\ 1 \end{bmatrix}, \quad \mathbf{R}^{(2)} = \begin{bmatrix} \left(-\frac{Ad^2}{3}\right)\left(gd - \frac{Q^2}{d^2} + \frac{2}{3}Ad\psi\right)^{-1} \\ 0 \\ 0 \\ 1 \end{bmatrix},$$

$$\mathbf{R}^{(3)} = \begin{bmatrix} 0 \\ 0 \\ 1 \\ 0 \end{bmatrix}, \quad \mathbf{R}^{(4)} = \begin{bmatrix} \gamma \\ \gamma\left[\frac{Q}{d} + \sqrt{gd + \frac{Ad^2}{3\gamma} + \frac{2}{3}Ad\psi}\right] \\ 0 \\ 1 \end{bmatrix}. \tag{2.7}$$

Since

$$\nabla\lambda_i(\mathbf{U})\cdot\mathbf{R}^{(i)}(\mathbf{U}) \neq 0, \forall \mathbf{U} \in \Re^m \quad \text{for} \quad i = 1,4, \tag{2.8}$$

and

$$\nabla\lambda_i(\mathbf{U})\cdot\mathbf{R}^{(i)}(\mathbf{U}) = 0, \forall \mathbf{U} \in \Re^m, \quad \text{for} \quad i = 2,3, \tag{2.9}$$

(where $\Re^m$ is the set of real-valued vectors of m components, called the phase space), the λ_1 and λ_4 characteristic fields are said to be genuinely nonlinear, while the λ_2 and λ_3 characteristic fields are said to be linearly degenerate. More details on the hyperbolic structure and on the dispersive character of the DNSWE can be found in [1].

3 Wave solutions for the Riemann problem

The solution of the Riemann problem for the DNSWE involves four waves: two waves are associated with the genuinely nonlinear eigenvalues λ_1 and λ_4 and can be shock waves or rarefaction waves, while the other two waves are associated with the linearly degenerate fields λ_2 and λ_3 and are two superimposed contact discontinuities lying on the t-axis. These four wave families separate four constant states denoted, from left to right, by $\mathbf{U}_L$, $\mathbf{U}_{*L}$, $\mathbf{U}_{*R}$ and $\mathbf{U}_R$. The types of non-linear left and right waves are determined by the

following entropy conditions:

$$\left.\begin{array}{lcl} \lambda_1(\mathbf{U}_L) > S_1 > \lambda_1(\mathbf{U}_{*L}) & : & \text{left wave is a shock wave,} \\ \lambda_1(\mathbf{U}_L) < \lambda_1(\mathbf{U}_{*L}) & : & \text{left wave is a rarefaction wave,} \\ \lambda_4(\mathbf{U}_{*R}) > S_4 > \lambda_4(\mathbf{U}_R) & : & \text{right wave is a shock wave,} \\ \lambda_4(\mathbf{U}_{*R}) < \lambda_4(\mathbf{U}_R) & : & \text{right wave is a rarefaction wave.} \end{array}\right\} \tag{3.1}$$

More details on the conditions satisfied by the different waves can be found in [8, 16].

3.1 Rarefaction waves

If the λ_i-wave is a rarefaction, we can apply the constancy of the generalized Riemann invariants:

$$\frac{dU_1}{R_1^{(i)}} = \frac{dU_2}{R_2^{(i)}} = \frac{dU_3}{R_3^{(i)}} = \cdots = \frac{dU_m}{R_m^{(i)}}, \tag{3.2}$$

and for a left rarefaction we get

$$\phi = \text{const.}, \qquad d_{*L} - \gamma\psi_{*L} = d_L - \gamma\psi_L = C_0 \tag{3.3}$$

and

$$\sqrt{b_1 d + b_2 d^2}\left\{1 + \frac{b_1}{2\sqrt{b_2}\sqrt{b_1 d + b_2 d^2}} \ln\left[\frac{b_1 + 2b_2 d}{2\sqrt{b_2}} + \sqrt{b_1 d + b_2 d^2}\right]\right\} + u = \text{const.}, \tag{3.4}$$

with

$$b_1 = \left(g - \frac{2}{3}\frac{C_0 A}{\gamma}\right) \qquad \text{and} \qquad b_2 = \frac{A}{\gamma}. \tag{3.5}$$

Eq. (3.4) can be summarized in the following form:

$$f(d, b_1, b_2) + u = \text{const.}, \tag{3.6}$$

i.e.,

$$u_L + f(d_L, \psi_L) = u_{*L} + f(d_{*L}, \psi_{*L}), \tag{3.7}$$

that is

$$u_{*L} = u_L - f_R(d_{*L}, d_L, \psi_L) \quad \text{with} \quad f_R(d_{*L}, d_L, \psi_L) = f(d_L, \psi_L) - f(d_{*L}, \psi_{*L}). \tag{3.8}$$

Note that ψ_{*L} can be expressed in terms of d_L, d_{*L} and ψ_L, according to Eq. (3.3).

Analogously, if the right wave is a rarefaction, by applying the constancy of the generalized Riemann invariants we obtain

$$\phi = \text{const.}, \qquad d_{*R} - \gamma\psi_{*R} = d_R - \gamma\psi_R = C_1 \tag{3.9}$$

and

$$f(d,b_2,b_3)-u=\text{const.}, \tag{3.10}$$

with

$$f(d,b_2,b_3)=\sqrt{b_3d+b_2d^2}\left\{1+\frac{b_3}{2\sqrt{b_2}\sqrt{b_3d+b_2d^2}}\ln\left[\frac{b_3+2b_2d}{2\sqrt{b_2}}+\sqrt{b_3d+b_2d^2}\right]\right\}, \tag{3.11}$$

and

$$b_3=\left(g-\frac{2}{3}\frac{C_1A}{\gamma}\right). \tag{3.12}$$

Eq. (3.10) can be summarized in the following form:

$$u_{*R}=u_R-f_R(d_{*R},d_R,\psi_R). \tag{3.13}$$

3.2 Shock waves

If the left wave is a shock, the Rankine-Hugoniot conditions

$$\mathbf{F}(\mathbf{U}_{*L})-\mathbf{F}(\mathbf{U}_L)=V_1(\mathbf{U}_{*L}-\mathbf{U}_L) \tag{3.14}$$

hold true across the discontinuity. In order to facilitate their application, we introduce a frame of reference moving with the shock speed V_L. Then the relative velocities are:

$$\hat{u}_L=u_L-V_L, \qquad \hat{u}_{*L}=u_{*L}-V_L. \tag{3.15}$$

By re-writing the original Rankine-Hugoniot conditions

$$Q_{*L}-Q_L=V_2(d_{*L}-d_L), \tag{3.16a}$$

$$\left[g\frac{d_{*L}^2}{2}+\frac{Q_{*L}^2}{d_{*L}}+\frac{Ad_{*L}^2}{3}\psi_{*L}\right]-\left[g\frac{d_L^2}{2}+\frac{Q_L^2}{d_L}+\frac{Ad_L^2}{3}\psi_L\right]=V_2(Q_{*L}-Q_L), \tag{3.16b}$$

$$0=V_2(\phi_{*L}-\phi_L), \tag{3.16c}$$

$$\frac{Q_{*L}}{\gamma}-\frac{Q_L}{\gamma}=V_2(\psi_{*L}-\psi_L) \tag{3.16d}$$

in the new reference frame, we get

$$\hat{u}_{*L}d_{*L}-\hat{u}_Ld_L=0, \tag{3.17a}$$

$$\left[g\frac{d_{*L}^2}{2}+\hat{u}_{*L}^2d_{*L}+\frac{Ad_{*L}^2}{3}\psi_{*L}\right]-\left[g\frac{d_L^2}{2}+\hat{u}_L^2d_L+\frac{Ad_L^2}{3}\psi_L\right]=0, \tag{3.17b}$$

$$0=V_2(\phi_{*L}-\phi_L), \tag{3.17c}$$

$$0=V_2\left[\psi_{*L}-\psi_L-\frac{d_{*L}-d_L}{\gamma}\right]. \tag{3.17d}$$

With some algebra, the following equation can be finally obtained:

$$u_{*L}=u_L-(d_{*L}-d_L)\sqrt{\frac{1}{d_{*L}d_L}\left\{\frac{1}{2}g(d_L+d_{*L})+\frac{A}{3}\left[\psi_L(d_L+d_{*L})+\frac{d_{*L}^2}{\gamma}\right]\right\}}, \tag{3.18}$$

(for details in the computation see [16]) or, in a more compact form:

$$u_{*L}=u_L-f_S(d_{*L},d_L,\psi_L), \tag{3.19}$$

with the obvious definition for f_S.

Analogously, if the right wave is a shock, we can apply the Rankine-Hugoniot conditions and obtain

$$u_{*R}=u_R+(d_{*R}-d_R)\sqrt{\frac{1}{d_{*R}d_R}\left\{\frac{1}{2}g(d_R+d_{*R})+\frac{A}{3}\left[\psi_R(d_R+d_{*R})+\frac{d_{*R}^2}{\gamma}\right]\right\}}, \tag{3.20}$$

or, in a more compact form:

$$u_{*R}=u_R+f_S(d_{*R},d_R,\psi_R). \tag{3.21}$$

3.3 Contact discontinuities

In the linearly degenerate fields $i=2$ and $i=3$, two coincident contact discontinuities are generated. If we superimpose the results obtained by applying both the constancy of the Riemann Invariants and the Rankine-Hugoniot conditions for $i=2$ and $i=3$, we finally get:

$$[F_1]=0, \quad \text{and} \quad [F_2]=0. \tag{3.22}$$

Since $\lambda_2=\lambda_3\equiv 0$, the contact discontinuity is always located at $x=0$, that is, along the t-axis.

4 Resonance in the solution

Thanks to a richer hyperbolic structure, the solution of the Riemann problem for the homogeneous DNSWE shows a behavior which is generally more complex than that of the NSWE. In particular a resonance phenomenon can occur when one of the genuinely nonlinear fields crosses the zero value. The resonance is, therefore, generated by the nonlinear interaction between the linearly degenerate field λ_3 and the genuinely nonlinear field crossing zero and is a consequence of a local lack of hyperbolicity of the system. However, as shown by Isaacson [9], the solution of the Riemann problem still preserves uniqueness and existence and can be represented in a "canonical way", that is, through shock waves, rarefaction waves and contact discontinuities. In this case the resonance is identified by a compound wave, that is, a wave made by a contact discontinuity and a

rarefaction fan joined together. Finally, we underline that the crossover of the zero value is only a necessary condition for the occurrence of the resonance and, therefore, proper conditions for the compound wave generation are needed.

Here we propose the solution of the Riemann problem for the DNSWE in a neighborhood of a state at which one of the nonlinear waves assumes a zero speed. According to the work of Isaacson and Temple [9], we can state that the nature of the wave interaction is given by the solution of the Riemann problem, which is proved to exist, to be unique and to have a fixed structure under some generic conditions on the fluxes.

In particular, the homogeneous part of the original set of the DNSWE (1.2) can be written in the following form (for the homogeneous problem the third equation is trivial and, therefore, will not be considered in the following):

$$\begin{cases} d_t+Q_x=0, \\ Q_t+\left(\dfrac{gd^2}{2}+\dfrac{Q^2}{d}+\dfrac{Ad^2}{3}\psi\right)_x=0, \\ \gamma\psi_t-d_t=0. \end{cases} \tag{4.1}$$

Eq. (4.1) reduces to the form suggested by Isaacson and Temple [9]:

$$\mathbf{U}_t+\mathbf{F}(\mathbf{U})_x=0, \quad \mathbf{U}=(\mathbf{W},K), \quad \mathbf{F}(\mathbf{U})=(\mathbf{G}(K,\mathbf{W}),0), \tag{4.2}$$

if we set:

$$\mathbf{W}=\begin{bmatrix} d \\ Q \end{bmatrix}, \quad \mathbf{G}=\begin{bmatrix} Q \\ \dfrac{gd^2}{2}+\dfrac{Q^2}{d}+\dfrac{Ad^2}{3}\dfrac{K+d}{\gamma} \end{bmatrix} \quad \text{and} \quad K=\gamma\psi-d. \tag{4.3}$$

The system:

$$\mathbf{W}_t+\mathbf{G}(K,\mathbf{W})_x=0 \tag{4.4}$$

is strictly hyperbolic for $\forall K$ and $d\neq 0$ (i.e., $\lambda_2<\lambda_1$). The Jacobian matrix of system (4.1) is:

$$\mathbf{J}=\begin{bmatrix} 0 & 1 & 0 \\ gd-\dfrac{Q^2}{d^2}+\dfrac{Ad^2}{\gamma}+\dfrac{2}{3}\dfrac{AdK}{\gamma} & 2\dfrac{Q}{d} & \dfrac{Ad^2}{3\gamma} \\ 0 & 0 & 0 \end{bmatrix}, \tag{4.5}$$

the eigenvalues are:

$$\lambda_1=\frac{Q}{d}-\sqrt{gd+\frac{Ad^2}{\gamma}+\frac{2}{3}\frac{AdK}{\gamma}}, \tag{4.6a}$$

$$\lambda_2\equiv\lambda_0=0, \tag{4.6b}$$

$$\lambda_3=\frac{Q}{d}+\sqrt{gd+\frac{Ad^2}{\gamma}+\frac{2}{3}\frac{AdK}{\gamma}}. \tag{4.6c}$$

The left and right eigenvectors are:

$$\mathbf{L}_1 = \begin{bmatrix} -\lambda_1\lambda_3 \\ \lambda_1 \\ \dfrac{Ad^2}{3\gamma} \end{bmatrix}, \quad \mathbf{L}_2 \equiv \mathbf{L}_0 = \begin{bmatrix} 0 \\ 0 \\ 1 \end{bmatrix}, \quad \mathbf{L}_3 = \begin{bmatrix} -\lambda_1\lambda_3 \\ \lambda_3 \\ \dfrac{Ad^2}{3\gamma} \end{bmatrix}, \tag{4.7a}$$

$$\mathbf{R}_1 = \begin{bmatrix} 1 \\ \lambda_1 \\ 0 \end{bmatrix}, \quad \mathbf{R}_2 \equiv \mathbf{R}_0 = \begin{bmatrix} \dfrac{Ad^2}{3\gamma} \\ 0 \\ \lambda_1\lambda_3 \end{bmatrix}, \quad \mathbf{R}_3 = \begin{bmatrix} 1 \\ \lambda_3 \\ 0 \end{bmatrix}. \tag{4.7b}$$

Note that we define as λ_0, $\mathbf{L}_0$ and $\mathbf{R}_0$ the eigenvalue and the left and right eigenvectors associated with the linearly degenerate field. Let us denote with $\bar{\mathbf{L}}_1,\cdots,\bar{\mathbf{L}}_n$ the left eigenvectors normalized so that $\bar{\mathbf{L}}_j\cdot\mathbf{R}_j=1$ for $j=1,\cdots,n$. We want to study the system (4.2) in a neighborhood of a state $\mathbf{U}_S=(K_S,\mathbf{W}_S)$ at which one of the nonlinear wave families of the system has a zero speed. Hence, we assume that:

$$\lambda_k(\mathbf{U}_S)=\lambda_0=0. \tag{4.8}$$

It is possible to demonstrate that, for the system under consideration, the following conditions are satisfied:

$$\nabla\lambda_k\cdot\mathbf{R}_k(\mathbf{U}_S)\neq 0 \tag{4.9}$$

and

$$\bar{\mathbf{L}}_k\cdot\mathbf{F}_K(\mathbf{U}_S)\neq 0 \tag{4.10}$$

(nondegeneracy assumption), where $\mathbf{F}_K$ is $\partial\mathbf{F}/\partial K$. As stated by Isaacson and Temple [9], assumptions (4.8), (4.9) and (4.10) guarantee that, in a neighborhood of the state $\mathbf{U}_S$, the Riemann problem has an unique solution with a canonical structure. In the specific, assumption (4.9) guarantees that equation $\lambda_k=0$ defines a smooth n-dimensional surface locally in $\mathfrak{R}^{n+1}$, which passes through the state $\mathbf{U}_S$ and which we call $\mathfrak{I}$. Since the eigenvector $\mathbf{R}_k$ points along the hyperplane $K=const$, condition (4.9) guarantees that the integral curve of $\mathbf{R}_k$ cuts the transition surface $\mathfrak{I}$ transversely. Condition (4.10), instead, implies that the $n\times(n+1)$ matrix $\partial\mathbf{G}/\partial\mathbf{W}$ has a maximal rank n at $\mathbf{W}_S$. Hence $\partial\mathbf{F}/\partial\mathbf{U}$ has the Jordan normal form for every $\mathbf{U}\in\mathfrak{I}$ in a neighborhood of $\mathbf{U}_S$, as the condition (4.10) is an open one. This also implies that the eigenvectors $\mathbf{R}_0$ and $\mathbf{R}_k$ can be chosen off $\mathfrak{I}$, so that they have smooth extensions that agree on $\mathfrak{I}$, i.e. $\mathbf{R}_0$ continues smoothly to $\mathbf{R}_k$ on $\mathfrak{I}$. Finally, condition (4.9) implies that the integral curves for both $\mathbf{R}_0$ and $\mathbf{R}_k$ cut the surface $\mathfrak{I}$ transversely near the state $\mathbf{U}_S$. In particular, the integral curves of $\mathbf{R}_0$ that pass through the states $\mathbf{U}_0\in\mathfrak{I}$ in a neighborhood of $\mathbf{U}_S$ do not cross the hyperplane $K=K_0$ at $\mathbf{U}_0$, but they must cross the hyperplane $K=const.$ exactly twice at values of K on one side of $K=K_0$ (see Fig. 2).

In conclusion, let us consider two generic constant states $\mathbf{U}_L$ and $\mathbf{U}_R$, lying respectively on the left and on the right of the contact discontinuity and on the same integral

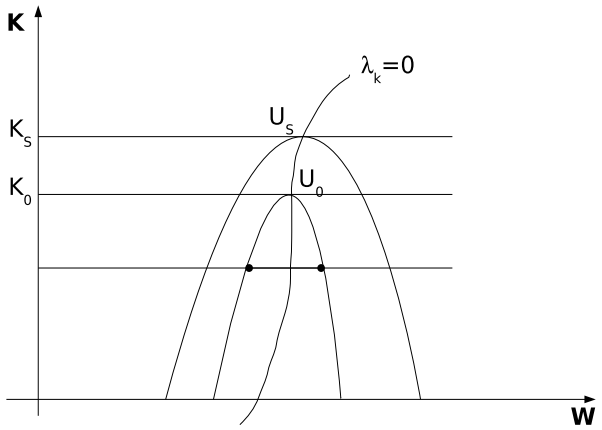

Figure 2: Sketch of the integral curves of $\mathbf{R}_0$ and of the surface $\mathfrak{I}$.

curve of $\mathbf{R}_0$. If the system was strictly hyperbolic, we would have expected a 0-wave (i.e. a wave of the family associated to the eigenvalue λ_0) coinciding with the integral curve of $\mathbf{R}_0$ to collect such states together. However, since the system (4.1) is not strictly hyperbolic when λ_k crosses the zero, a 0-wave that connects them on the same integral curve of $\mathbf{R}_0$ by a contact discontinuity of speed zero is admissible only if the integral curve of $\mathbf{R}_0$ does not cross the transitional surface $\mathfrak{I}$ between $\mathbf{U}_L$ and $\mathbf{U}_R$. Otherwise, if the 0-wave coincided with the integral curve, we would have the generation of inadmissible shocks, like the rarefaction shock shown in Fig. 3, where $\lambda_k(\mathbf{U}_L<0)$ and $\lambda_k(\mathbf{U}_R)>0$. As a consequence, the 0-wave cannot coincide with the integral curve itself, but it interacts with the k-wave (i.e. the wave associated to the eigenvalue λ_k) and gives rise to a compound wave (see [9]).

Using all this information, it is possible to construct the solution of the Riemann problem in a neighborhood of the state $\mathbf{U}_S$. In the following, we assume the existence of a state at which $\lambda_1=0$ and analyze the construction of the solution of the Riemann problem for the homogeneous DNSWE (2.1) in detail. In particular, recall that, if both the states $\mathbf{U}_{*R}$ and $\mathbf{U}_R$ lie on the surface $K=K_R$, the 4-wave connecting them has to move on such a surface and the 0-wave cannot be traveled over anymore. For this reason, the behaviour of the solution is not affected by a new change in the sign of the eigenvalue λ_1, while passing through the 4-wave.

Here we show the solution of some typical cases containing a state at which $\lambda_1=0$. For the sake of simplicity, the eigenvalue λ_4 is assumed to be always positive.

Example 4.1. If

$$K_L>K_R \quad \text{and} \quad \begin{cases} \lambda_1(\mathbf{U}_L)<0, \\ \lambda_1(\mathbf{U}_{*L})>0, \\ \lambda_1(\mathbf{U}_{*R})>0, \end{cases} \tag{4.11}$$

the solution exhibits the pattern shown in Fig. 4. The 1-wave interacts with the 0-wave on

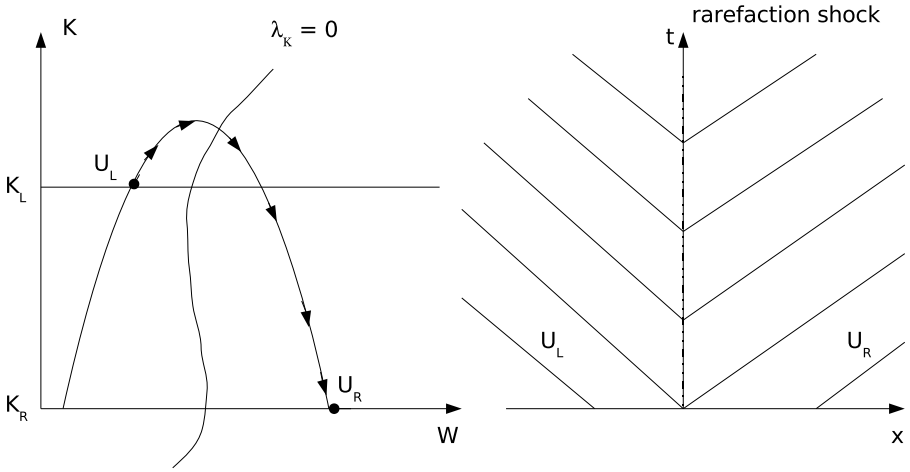

Figure 3: If the 0-wave that connects the two states $\mathbf{U}_L$ and $\mathbf{U}_R$ coincides with the integral curve, an inadmissible rarefaction shock is generated.

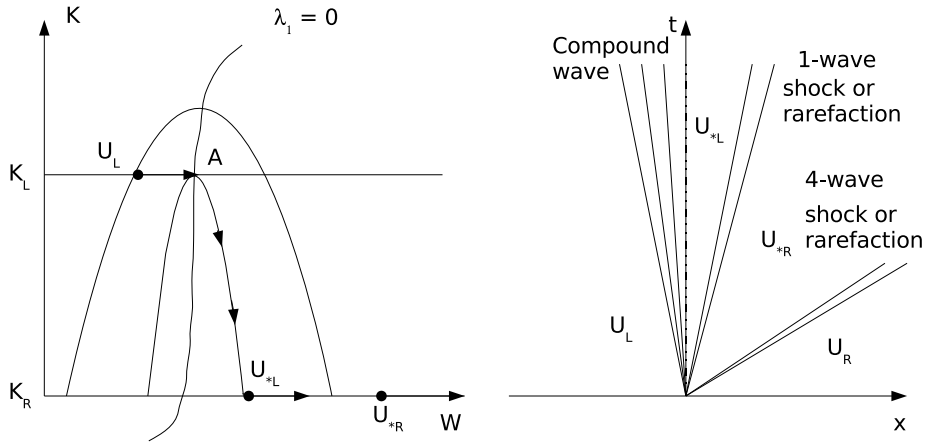

Figure 4: Wave pattern in Example 4.1: the 1-wave and the 0-wave interact giving rise to a resonant behaviour of the solution on the left of the contact discontinuity.

the left of the contact discontinuity, giving rise to a rarefaction fan attached to a contact discontinuity: in fact, as in A the $\mathbf{R}_1$ eigenvector coincides with the $\mathbf{R}_0$ one, the 1-wave is smoothly connected to the 0-wave, giving rise to a unique path, called compound wave. To see it, recall that the 0-wave coincides with the integral curve of $\mathbf{R}_0$; moreover, in A the 1-wave coincides locally with the integral curve of $\mathbf{R}_1$, λ_1 being equal to zero. Therefore, in A the 1-wave is locally superimposed to the 0-wave and the transition between the two waves is smooth. Hence moving from the left state $\mathbf{U}_L$ to the right state $\mathbf{U}_{*R}$ we encounter a rarefaction fan immediately followed by a contact discontinuity (the compound wave), the constant state ($\mathbf{U}_{*L}$) and a rarefaction or a shock 1-wave. The constant state ($\mathbf{U}_{*R}$), the rarefaction or shock 4-wave and the right constant state ($\mathbf{U}_R$) follow.

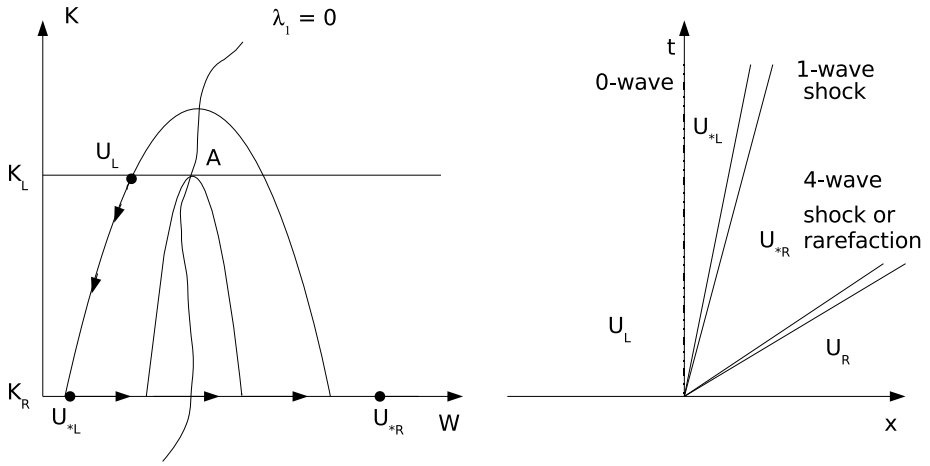

Figure 5: Wave pattern in Example 4.2: no interaction between the 1-wave and the 0-wave.

Example 4.2. If

$$K_L > K_R \quad \text{and} \quad \begin{cases} \lambda_1(\mathbf{U}_L) > 0, \\ \lambda_1(\mathbf{U}_{*L}) > 0, \\ \lambda_1(\mathbf{U}_{*R}) < 0, \end{cases} \tag{4.12}$$

the solution exhibits the pattern shown in Fig. 5. In this case, the solution does not present a resonant behavior, as the 1-wave does not interact with the 0-wave. In fact, as $\lambda_1(\mathbf{U}_L) > 0$ and $\lambda_1(\mathbf{U}_{*L}) > 0$, the solution is forced to encounter the 0-wave first, without passing through the interaction point A. The $\mathbf{U}_{*L}$ constant state, the shock 1-wave, the $\mathbf{U}_{*R}$ constant state, the rarefaction or shock 4-wave and the right constant state $\mathbf{U}_R$ follow. Since $\lambda_1(\mathbf{U}_{*L}) > \lambda_1(\mathbf{U}_{*R})$, the 1-wave is forced to be a shock.

Example 4.3. If

$$K_R > K_L \quad \text{and} \quad \begin{cases} \lambda_1(\mathbf{U}_L) < 0, \\ \lambda_1(\mathbf{U}_{*L}) < 0, \\ \lambda_1(\mathbf{U}_{*R}) > 0, \end{cases} \tag{4.13}$$

the solution exhibits the pattern shown in Fig. 6. The 1-wave interacts with the 0-wave on the right of the contact discontinuity, giving rise to a contact discontinuity attached to a rarefaction fan. In fact, as $\lambda_1(\mathbf{U}_L) < 0$ and $\lambda_1(\mathbf{U}_{*L}) < 0$, the solution is forced to encounter the rarefaction or shock 1-wave first, reaching the constant state $\mathbf{U}_{*L}$. Then it moves on the 0-wave, until it passes through the interaction point A, where the path smoothly moves on the 1-wave again, until the $\mathbf{U}_{*R}$ constant state is reached. Incidentally, we note that if we assume $\lambda_1(\mathbf{U}_L) > 0$, the solution pattern is the same shown in Fig. 6. In fact, as a consequence of the entropy condition in (3.1), the 1-wave connecting $\mathbf{U}_L$ and $\mathbf{U}_{*L}$ is a shock with speed $S < 0$. This implies that the constant state $\mathbf{U}_{*L}$ must lie on the plane $K = K_L$.

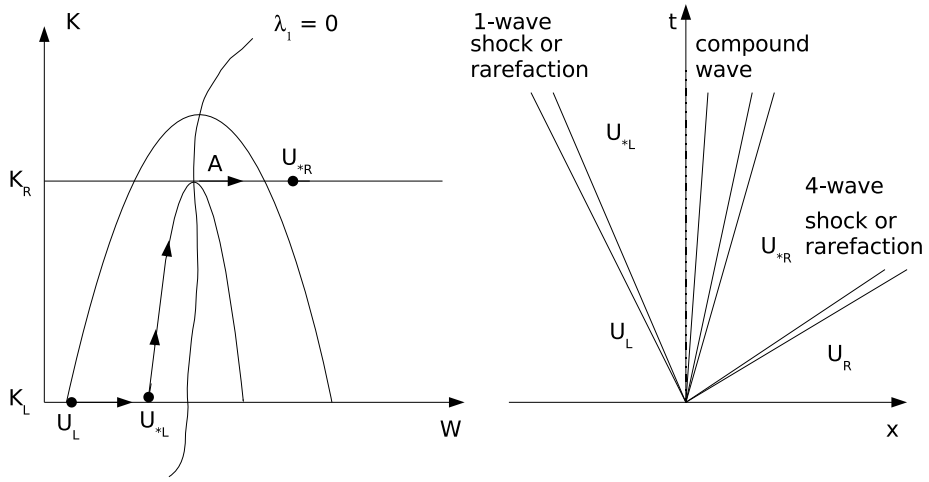

Figure 6: Wave pattern in Example 4.3: the 1-wave and the 0-wave interact giving rise to a resonant behaviour of the solution on the right of the contact discontinuity.

Example 4.4. If

$$K_R > K_L \quad \text{and} \quad \begin{cases} \lambda_1(\mathbf{U}_L) > 0, \\ \lambda_1(\mathbf{U}_{*L}) > 0, \\ \lambda_1(\mathbf{U}_{*R}) < 0, \end{cases} \tag{4.14}$$

the solution exhibits the pattern shown in Fig. 7. In this case, the solution does not present a resonant behaviour, as the 1-wave does not interact with the 0-wave. In fact, as $\lambda_1(\mathbf{U}_L) > 0$ and $\lambda_1(\mathbf{U}_{*L}) > 0$, the solution is forced to encounter the 0-wave first. After the plane $K = K_R$ is reached, the 0-wave cannot be traveled anymore. As a consequence there is no interaction between the 1-wave and the 0-wave in the point A. The $\mathbf{U}_{*L}$ constant state, the shock 4-wave and the $\mathbf{U}_{*R}$ constant state follow. Notice that, as $\lambda_1(\mathbf{U}_{*L}) > \lambda_1(\mathbf{U}_{*R})$ the 1-wave is forced to be a shock.

Example 4.5. If

$$K_R > K_L \quad \text{and} \quad \begin{cases} \lambda_1(\mathbf{U}_L) < 0, \\ \lambda_1(\mathbf{U}_{*L}) < 0, \\ \lambda_1(\mathbf{U}_{*R}) > 0, \end{cases} \tag{4.15}$$

the solution presents the pattern shown in Fig. 8. In this resonant case, the two states $\mathbf{U}_L$ and $\mathbf{U}_{*R}$ cannot be connected by the same 0-wave; hence the solution moves through a 1-wave towards the intermediate 0-wave that encounters the transition interface on the hyperplane K_R. Here we find the constant state $\mathbf{U}_{*L}$. In the interaction point A, the contact discontinuity and the rarefaction 1-wave are smoothly connected and the solution reaches the constant state $\mathbf{U}_{*R}$. If $\lambda_1(\mathbf{U}_L) > 0$, the solution exhibits the same pattern shown in Fig. 8. In fact the 1-wave connecting $\mathbf{U}_L$ and $\mathbf{U}_{*L}$ is a shock with speed $S < 0$.

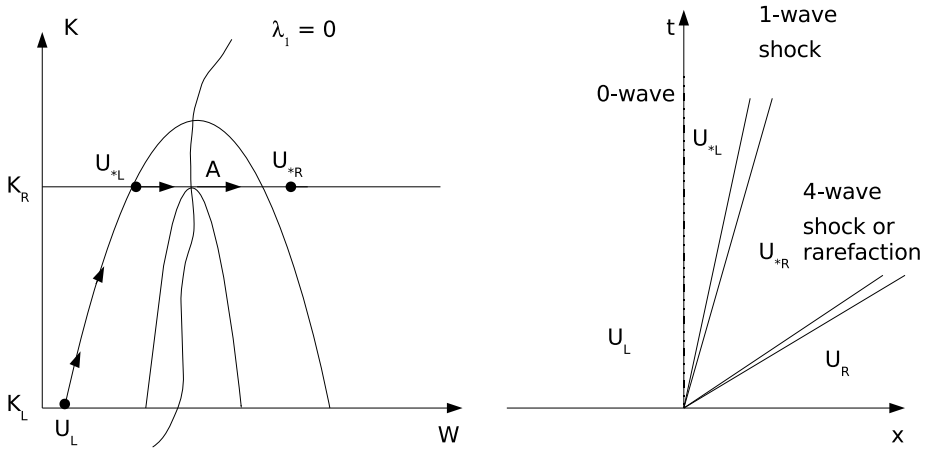

Figure 7: Wave pattern in Example 4.4: no interaction between the 1-wave and the 0-wave.

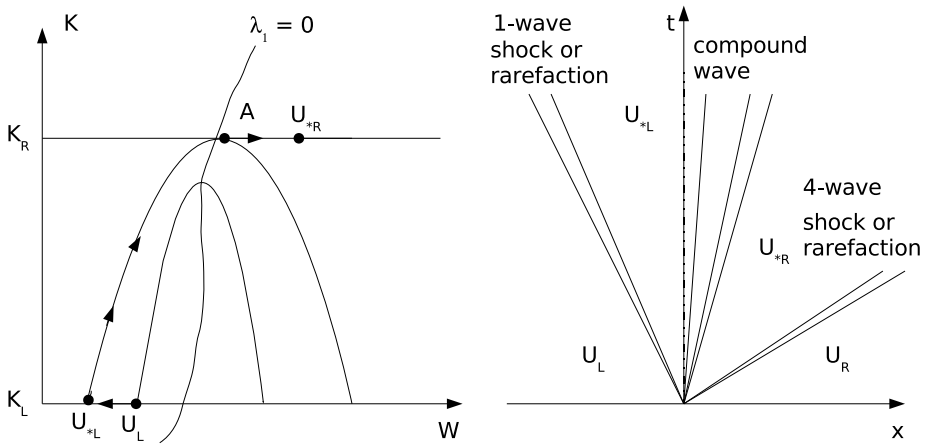

Figure 8: Wave pattern in Example 4.5: the 1-wave and the 0-wave interact giving rise to a resonant behaviour of the solution on the right of the contact discontinuity.

Example 4.6. If

$$K_R > K_L \quad \text{and} \quad \begin{cases} \lambda_1(\mathbf{U}_L) > 0, \\ \lambda_1(\mathbf{U}_{*L}) < 0, \\ \lambda_1(\mathbf{U}_{*R}) < 0, \end{cases} \tag{4.16}$$

the solution presents the pattern shown in Fig. 9. In this case, the solution does not present a resonant behaviour, as the 1-wave, moving on the surface $K = K_L$, does not interact with the 0-wave. The 1-wave is necessarily a shock one, as $\lambda_1(\mathbf{U}_L) > \lambda_1(\mathbf{U}_{*L})$. The $\mathbf{U}_{*L}$ constant state, the contact discontinuity and the $\mathbf{U}_{*R}$ constant state follow.

Example 4.7. If

$$K_R = K_L \quad \text{and} \quad \begin{cases} \lambda_1(\mathbf{U}_L) < 0, \\ \lambda_1(\mathbf{U}_{*L}) > 0, \end{cases} \tag{4.17}$$

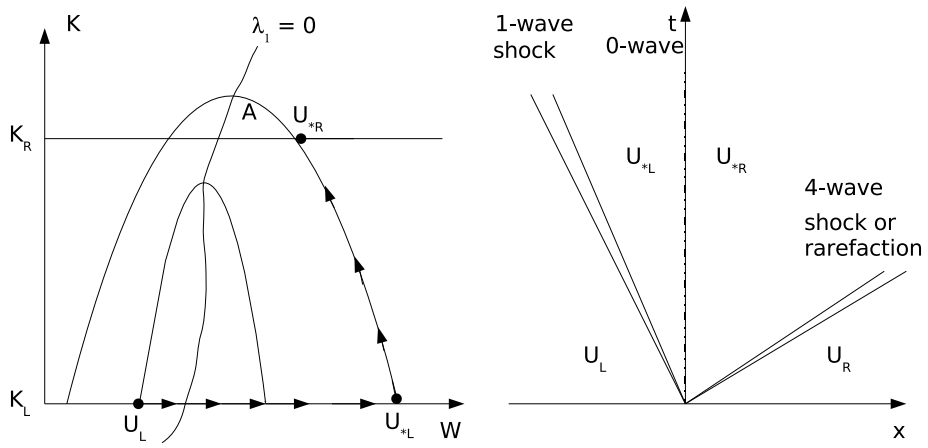

Figure 9: Wave pattern in Example 4.6: no interaction between the 1-wave and the 0-wave.

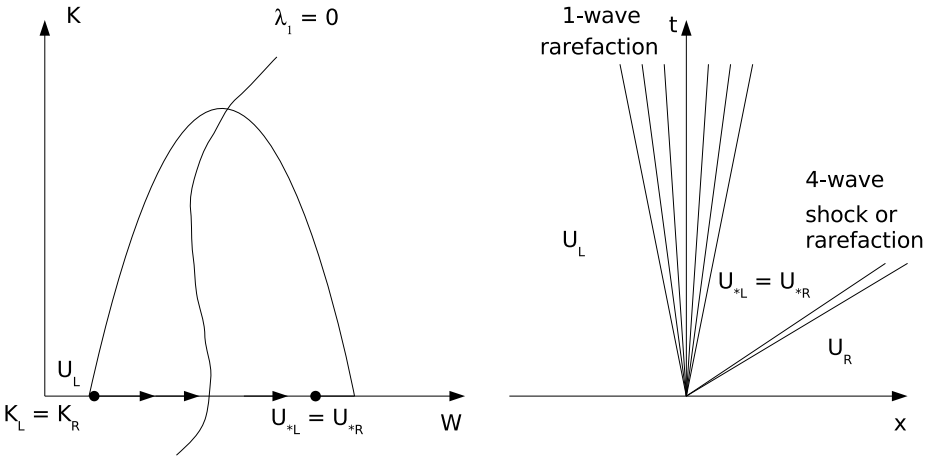

Figure 10: Wave pattern in Example 4.7: The 1-rarefaction wave crosses the t-axis without any interaction with the 0-wave.

the solution presents the pattern shown in Fig. 10. In this case, the solution does not present a resonant behaviour. In fact, as $K_R = K_L$, the contact discontinuity vanishes and the rarefaction crosses the t-axis, without any interaction with the 0-wave. When $K_R = K_L$, the solution pattern of the DNSWE reduces to the one of the classical Nonlinear Shallow Water Equations.

Example 4.8. If

$$K_R = K_L \quad \text{and} \quad \begin{cases} \lambda_1(\mathbf{U}_L) > 0 \\ \lambda_1(\mathbf{U}_{*L}) < 0, \end{cases} \tag{4.18}$$

the solution presents the pattern shown in Fig. 11. In this case, the solution does not present a resonant behaviour. In fact, as $K_R = K_L$, the contact discontinuity vanishes and the shock can lie on the left or over the t-axis, without any interaction with the 0-wave.

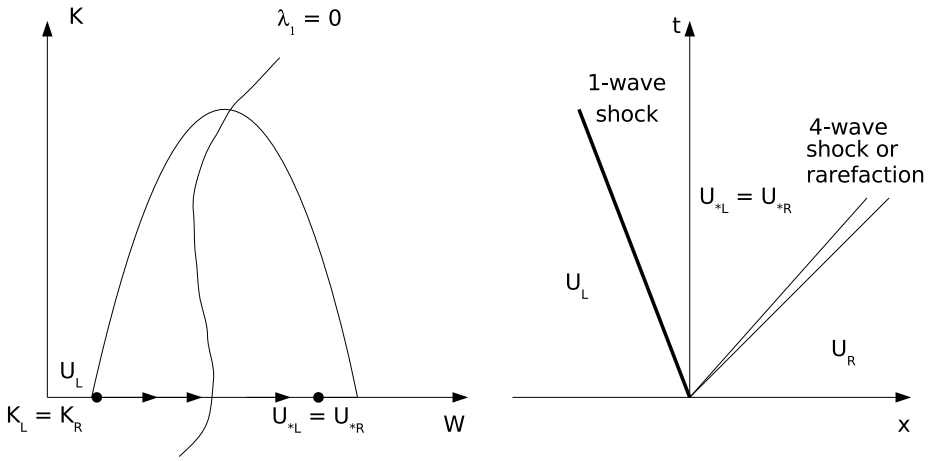

Figure 11: Wave pattern in Example 4.8: The 1-shock wave lies on the left of t-axis without any interaction with the 0-wave.

In Table 1 we give a summary of the examples explained above. It can be seen that different combinations of the eigenvalue signs coupled with the relation between K_L and K_R can give rise to different wave patterns, determining wether the resonance occurs or not and its position with respect to the t-axis.

Table 1: Summary of the examples of the wave patterns obtained with different combinations of the eigenvalue signs.

Example	K	$\lambda(\mathbf{U}_L)$	$\lambda(\mathbf{U}_{*L})$	$\lambda(\mathbf{U}_{*R})$	resonance
1	$K_L > K_R$	-	+	+	yes
2	$K_L > K_R$	+	+	-	no
3	$K_L < K_R$	-	-	+	yes
4	$K_L < K_R$	+	+	-	no
5	$K_L < K_R$	-	-	+	yes
6	$K_L < K_R$	+	-	-	no
7	$K_L = K_R$	-	+	+	no
8	$K_L = K_R$	+	-	-	no

5 A solution strategy

On the basis of what we have explained above, we can state that the solution of the Riemann problem exhibits different wave patterns according to the reciprocal position of the discontinuities. In particular, in the previous section we have shown that a remarkable number of different configurations can be found when the two eigenvalues λ_1 and λ_4 change their sign. Moreover, when the two eigenvalues λ_1 and λ_4 remain positive or negative, we can also have two different configurations: the basic one, in which the

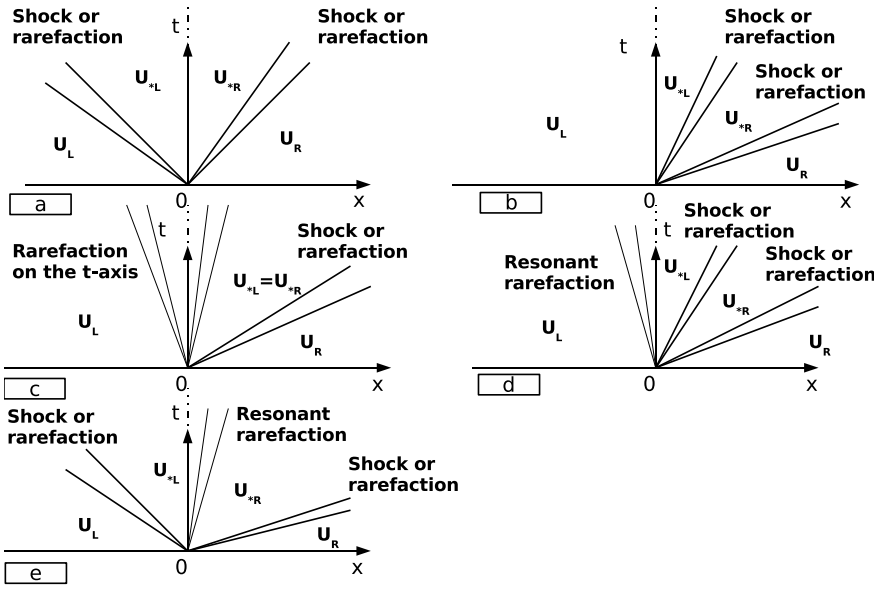

Figure 12: Possible wave patterns in the solution of the Riemann problem for the dispersive nonlinear shallow water equations.

eigenvalue λ_1 is always negative, while the eigenvalue λ_4 is always positive and the one in which both the two eigenvalues λ_1 and λ_4 are positive or negative. In the former case, the two waves associated with the eigenvalues λ_1 and λ_4 lie respectively on the left and on the right of the t-axis, while in the latter one, both the waves associated with the eigenvalues λ_1 and λ_4 lie on the same side of the t-axis. All these cases, including the resonant ones, can be summarized as shown in Fig. 12, where one half of the possible configurations is represented (the other-half is represented by the symmetrical cases). Notice that 'Configuration a' does not need a symmetrical one.

In the following we present a complete description of all the possible configurations and the conditions for their occurrence. Since such conditions depend on the solution itself (i.e. on $\mathbf{U}_{*L}$ and $\mathbf{U}_{*R}$), a set of trial values is needed to detect the correct configuration and solve the equations valid in it. The trial values can be obtained by using an approximate numerical solver (like a Rusanov one). After getting the analytical solution of the equations valid in the chosen configuration, it is necessary to verify wether these values satisfy the conditions for the occurrence of the configuration itself. If they do not, the correct configuration has to be considered and a new solution has to be found. Hence, the solution is based on an iterative procedure.

5.1 Configuration a

In this configuration, the left and the right rarefaction or shock waves lie respectively on the left and on the right of the t-axis, while the two contact discontinuities coincide and

lie exactly on the t-axis. This configuration takes place, for example, in the basic case in which the eigenvalue λ_1 is always negative and the eigenvalue λ_4 is always positive or in the case shown in Example 4.6 of Section 4. In general, this wave pattern occurs when the following conditions are satisfied:

$$\lambda_1(\mathbf{U}_{*L})<0 \quad \text{and} \quad \lambda_1(\mathbf{U}_{*R})<0, \tag{5.1a}$$

$$\lambda_4(\mathbf{U}_{*L})>0 \quad \text{and} \quad \lambda_4(\mathbf{U}_{*R})>0. \tag{5.1b}$$

In order to get the solution of the Riemann problem, we have to write the equations valid through every wave of the pattern. In particular, for the left and right waves, equations (3.8), (3.13), (3.19) and (3.21) apply:

$$\begin{array}{ll} u_{*L}=u_L-f_S(d_{*L},d_L,\psi_L) \quad \text{if} \quad \lambda_1(\mathbf{U}_L)>S_2>\lambda_1(\mathbf{U}_{*L}), & \left.\begin{array}{l}\\ \\ \end{array}\right\} \quad \text{left wave} \\ u_{*L}=u_L-f_R(d_{*L},d_L,\psi_L) \quad \text{if} \quad \lambda_1(\mathbf{U}_L)<\lambda_1(\mathbf{U}_{*L}), & \\ u_{*R}=u_R+f_S(d_{*R},d_R,\psi_R) \quad \text{if} \quad \lambda_4(\mathbf{U}_{*R})>S_1>\lambda_4(\mathbf{U}_R), & \left.\begin{array}{l}\\ \\ \end{array}\right\} \quad \text{right wave} \\ u_{*R}=u_R-f_R(d_{*R},d_R,\psi_R) \quad \text{if} \quad \lambda_4(\mathbf{U}_{*R})<\lambda_4(\mathbf{U}_R); & \end{array} \tag{5.2}$$

with

$$\psi_{*L}=\psi_L+\frac{d_{*L}-d_L}{\gamma}, \quad \psi_{*R}=\psi_R+\frac{d_{*R}-d_R}{\gamma}, \tag{5.3a}$$

$$\phi_{*L}=\phi_L, \qquad \phi_{*R}=\phi_R. \tag{5.3b}$$

Moreover across the λ_2 and λ_3 discontinuities, the following conditions hold:

$$[F_1]=0, \iff u_{*L}d_{*L}=u_{*R}d_{*R}, \tag{5.4}$$

$$[F_2]=0, \iff \frac{gd_{*R}^2}{2}+\frac{(u_{*R}d_{*R})^2}{d_{*R}}+\frac{Ad_{*R}^2}{3}\psi_{*R}=\frac{gd_{*L}^2}{2}+\frac{(u_{*L}d_{*L})^2}{d_{*L}}+\frac{Ad_{*L}^2}{3}\psi_{*L}. \tag{5.5}$$

Using the above equations for u_{*L} and u_{*R} and adding Eqs. (5.4) and (5.5), we obtain a set of four equations in the four unknowns d_{*L}, d_{*R}, u_{*L} and u_{*R}:

$$\begin{cases} u_{*L}=u_L-f_{R,S}(d_{*L},d_L,\psi_L), \\ u_{*R}=u_R\mp f_{R,S}(d_{*R},d_R,\psi_R), \\ u_{*L}d_{*L}=u_{*R}d_{*R}, \\ \dfrac{gd_{*R}^2}{2}+\dfrac{(u_{*R}d_{*R})^2}{d_{*R}}+\dfrac{Ad_{*R}^2}{3}\left[\psi_R+\dfrac{d_{*R}-d_R}{\gamma}\right] \\ \quad =\dfrac{gd_{*L}^2}{2}+\dfrac{(u_{*L}d_{*L})^2}{d_{*L}}+\dfrac{Ad_{*L}^2}{3}\left[\psi_L+\dfrac{d_{*L}-d_L}{\gamma}\right], \end{cases} \tag{5.6}$$

where the choice of f_R or f_S for u_{*L} and u_{*R} depends on the solution itself. Such a system of equations can be solved by using a standard multivariate Newton method for non-linear systems of equations as described, e.g. in Chapter 9.7 of [13]. After calculating d_{*L}, d_{*R}, u_{*L} and u_{*R}, the quantities ϕ_{*L}, ϕ_{*R}, ψ_{*L} and ψ_{*R} can be also obtained by using Eq. (5.3).

5.2 Configuration b

In this configuration, both the waves associated with the eigenvalues λ_1 and λ_4 lie on the right of the t-axis, while the two contact discontinuities coincide and lie exactly on the t-axis. This configuration can take place, for example, in the cases shown in Examples 4.2 and 4.9 of Section 4 or in the case in which both the two eigenvalues λ_1 and λ_4 are positive. In general, this wave pattern occurs when the following conditions are satisfied:

$$\lambda_1(\mathbf{U}_L)>0 \quad \text{and} \quad \lambda_1(\mathbf{U}_{*L})>0, \tag{5.7a}$$
$$\lambda_4(\mathbf{U}_{*L})>0 \quad \text{and} \quad \lambda_4(\mathbf{U}_{*R})>0. \tag{5.7b}$$

Across the λ_1 discontinuity the following equations apply:

$$\psi_{*L}=\psi_{*R}+\frac{(d_{*L}-d_{*R})}{\gamma}, \tag{5.8a}$$
$$u_{*R}=u_{*L}-f_{R,S}(d_{*R},d_{*L}), \tag{5.8b}$$

while across the λ_4 discontinuity the following equations hold:

$$\psi_{*R}=\psi_R+\frac{(d_R-d_R)}{\gamma}, \tag{5.9a}$$
$$u_R=u_R\mp f_{R,S}(d_{*R},d_R). \tag{5.9b}$$

Across the λ_2 and λ_3 discontinuities, we have:

$$[Q]=0, \iff u_L d_L=u_{*L}d_{*L}, \tag{5.10}$$
$$[F]=0, \iff \frac{gd_L^2}{2}+\frac{(u_L d_L)^2}{d_L}+\frac{Ad_L^2}{3}\psi_L=\frac{gd_{*L}^2}{2}+\frac{(u_{*L}d_{*L})^2}{d_{*L}}+\frac{Ad_{*L}^2}{3}\psi_{L*}. \tag{5.11}$$

Eqs. (5.8b), (5.9b), (5.10) and (5.11) can be rearranged in a system of four equations for the four unknowns d_{*L}, d_{*R}, u_{*L} and u_{*R}. Eqs. (5.8a) and (5.9a) can be used to find ψ_{*L} and ψ_{*R}. Notice that ϕ_{*L} is always equal to ϕ_L and ϕ_{*R} is always equal to ϕ_R.

5.3 Configuration c

In this configuration, the two contact discontinuities vanish and the left rarefaction wave lies on the t-axis, without any resonant behaviour, while the right rarefaction or shock wave is located on the right of it. This configuration can take place in situations analogous to the one shown in Example 4.7 of Section 4. In general, this wave pattern occurs when the following conditions are satisfied:

$$\left.\begin{array}{llllll}\lambda_1(\mathbf{U}_L)\le 0 & \text{and} & \lambda_1(\mathbf{U}_{*L})\ge 0 & \text{and} & \lambda_1(\mathbf{U}_{*R})\ge 0, \\ \lambda_4(\mathbf{U}_{*L})>0 & \text{and} & \lambda_4(\mathbf{U}_{*R})>0 & \text{and} & \lambda_4(\mathbf{U}_R)>0, \end{array}\right\} \quad \text{if} \quad K_L=K_R. \tag{5.12}$$

Across the λ_1 discontinuity the following equations apply:

$$\psi_{*L} = \psi_L + \frac{(d_{*L} - d_L)}{\gamma}, \tag{5.13a}$$

$$u_{*L} = u_L - f_R(d_{*L}, d_L), \tag{5.13b}$$

while across the and λ_4 discontinuity the following equations hold:

$$\psi_{*R} = \psi_R + \frac{(d_R - d_R)}{\gamma}, \tag{5.14a}$$

$$u_{*R} = u_R \mp f_{R,S}(d_{*R}, d_R). \tag{5.14b}$$

Moreover, we have that:

$$\psi_{*L} = \psi_{*R}, \tag{5.15a}$$

$$d_{*L} = d_{*R}, \qquad u_{*L} = u_{*R}. \tag{5.15b}$$

Eqs. (5.13b), (5.14b) and (5.15b) can be rearranged in a system of four equations for the four unknowns d_{*L}, d_{*R}, u_{*L} and u_{*R}. Eqs. (5.13a) and (5.15a) provide solutions for ψ_{*L} and ψ_{*R}.

5.4 Configuration d

In this configuration, the 1-wave interacts with the 0-wave, giving rise to a rarefaction attached to a contact discontinuity on the left of the t-axis (compound wave), followed by the constant state $\mathbf{U}_{*L}$. The latter is split from the $\mathbf{U}_{*R}$ state by the 1-rarefaction or shock wave. The right rarefaction or shock 1-wave lies on the right of the t-axis. This configuration can take place, for example in situations like the one shown in Example 4.1 of Section 4. In general, this wave pattern occurs when the following conditions are satisfied:

$$\left.\begin{array}{lll} \lambda_1(\mathbf{U}_L) < 0 & \text{and} & \lambda_1(\mathbf{U}_{*L}) > 0, \\ \lambda_4(\mathbf{U}_{*L}) > 0 & \text{and} & \lambda_4(\mathbf{U}_{*R}) > 0, \end{array}\right\} \quad \text{if} \quad K_L > K_R. \tag{5.16}$$

To solve this configuration, it is necessary to choose a point B very close to the t-axis, but on the left side of it (see Fig. 13). Since

$$\psi_{*L} = \psi_{*R} + \frac{1}{\gamma}(d_{*L} - d_{*R}), \quad \text{and} \quad \psi_{*R} = \psi_R + \frac{1}{\gamma}(d_{*R} - d_R), \tag{5.17}$$

we have that:

$$\psi_{*L} = \psi_R + \frac{1}{\gamma}(d_{*L} - d_R). \tag{5.18}$$

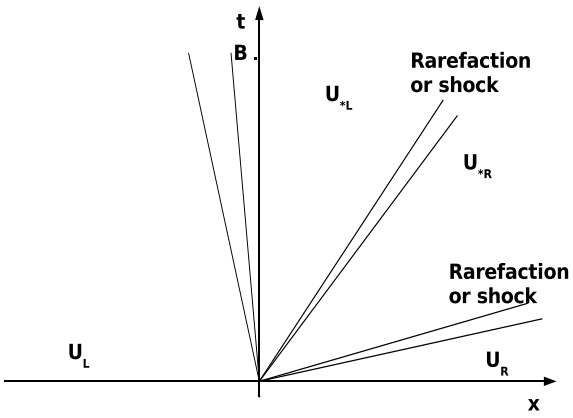

Figure 13: The wave pattern when the compound wave lies on the left of the t-axis.

Choosing $S_B = x_B/t_B$, with $S_B < 0$ and $|S_B| \ll 1$, the following conditions hold:

$$S_B = u_B - \sqrt{g d_B + \frac{A(d_B^2)}{3\gamma} + \frac{2}{3} A d_B \psi_B}, \tag{5.19a}$$

$$u_B = u_L - f_R(d_B, d_L, \psi_L), \tag{5.19b}$$

$$u_B d_B = u_{*L} d_{*L}, \tag{5.19c}$$

$$u_{*L} = u_{*R} - f_{R,S}(d_{*L}, d_{*R}), \tag{5.19d}$$

$$\frac{g d_B^2}{2} + \frac{(u_B d_B)^2}{d_B} + \frac{A d_B^2}{3}\psi_B = \frac{g d_{*L}^2}{2} + \frac{(u_{*L} d_{*L})^2}{d_{*L}} + \frac{A d_{*L}^2}{3}\psi_{*L}, \tag{5.19e}$$

with

$$\psi_B = \psi_L + \frac{1}{\gamma}(d_B - d_L), \tag{5.20}$$

while across the λ_4 shock or rarefaction wave, the following equations apply:

$$\psi_{*R} = \psi_R + \frac{(d_R - d_R)}{\gamma}, \tag{5.21a}$$

$$u_{*R} = u_R \mp f_{R,S}(d_{*R}, d_R). \tag{5.21b}$$

Eqs. (5.19) and (5.21b) can be set in a system of six equations for the six unknowns d_B, d_{*L}, d_{*R}, u_B, u_{*L} and u_{*R}; ψ_B, ψ_{*L} and ψ_{*R} can be obtained through Eqs. (5.18), (5.20) and (5.21a).

5.5 Configuration e

In this configuration, the 1-wave interacts with the 0-wave, giving rise to a contact discontinuity attached to a rarefaction on the right of the t-axis (compound wave). The constant

state $\mathbf{U}_{*L}$ is located on the left of the t-axis, split from the $\mathbf{U}_L$ state by the 1-rarefaction or shock wave. The compound wave is followed by the constant state $\mathbf{U}_{*R}$ and the right rarefaction or shock wave. This configuration can take place, for example in situations like the ones shown in Examples 4.3 and 4.5 in Section 4. In general, this wave pattern occurs when the following conditions are satisfied:

$$\left.\begin{array}{lll} \lambda_1(\mathbf{U}_{*L})<0 & \text{and} & \lambda_1(\mathbf{U}_{*R})>0, \\ \lambda_4(\mathbf{U}_{*L})>0 & \text{and} & \lambda_4(\mathbf{U}_{*R})>0, \end{array}\right\} \quad \text{if} \quad K_R>K_L. \tag{5.22}$$

To solve this configuration, it is possible to use the same strategy of 'Configuration d', after moving the point B on the right of the t axis, the rarefaction of the compound wave lying on the right side of it. In particular, we have that:

$$\psi_{*L}=\psi_L+\frac{1}{\gamma}(d_{*L}-d_L), \tag{5.23a}$$

$$\psi_B=\psi_{*R}+\frac{1}{\gamma}(d_B-d_{*R})=\psi_R+\frac{1}{\gamma}(d_B-d_R). \tag{5.23b}$$

Assuming that $S_B=x_B/t_B$, the following conditions hold:

$$S_B=u_B-\sqrt{gd_B+\frac{A(d_B^2)}{3\gamma}+\frac{2}{3}Ad_B\psi_B}, \tag{5.24a}$$

$$u_B=u_{*R}-f_R(d_B,d_{*R}), \tag{5.24b}$$

$$u_Bd_B=u_{*L}d_{*L}, \tag{5.24c}$$

$$u_{*L}=u_L-f_{R,S}(d_{*L},d_L), \tag{5.24d}$$

$$\frac{gd_B^2}{2}+\frac{(u_Bd_B)^2}{d_L}+\frac{Ad_B^2}{3}\psi_B=\frac{gd_{*L}^2}{2}+\frac{(u_{*L}d_{*L})^2}{d_{*L}}+\frac{Ad_{*L}^2}{3}\psi_{*L}, \tag{5.24e}$$

while across the λ_4 shock or rarefaction wave, the following equations apply:

$$\psi_{*R}=\psi_R+\frac{(d_{*R}-d_R)}{\gamma}, \tag{5.25a}$$

$$u_{*R}=u_R\mp f_{R,S}(d_{*R},d_R). \tag{5.25b}$$

Eqs. (5.24) and (5.25b) can be set in a system of six equations for the six unknowns d_B, d_{*L}, d_{*R}, u_B, u_{*L} and u_{*R}; ψ_B, ψ_{*L} and ψ_{*R} can be obtained through Eqs. (5.23) and (5.25a).

6 Sampling the solution

According to what explained in the previous sections, the solution in the constant regions $\mathbf{U}_L$, $\mathbf{U}_R$, $\mathbf{U}_{*L}$ and $\mathbf{U}_{*R}$ can be found by solving systems of nonlinear equations. Notice that the wave pattern, which establishes the equations to be solved, depends on the solution itself; hence the procedure to obtain the solution in the star regions must be iterative.

After calculating the solution in the constant state regions $\mathbf{U}_{*L}$ and $\mathbf{U}_{*L}$, it is possible to sample the solution in the whole domain. In particular, to find the solution in a rarefaction fan (for example the left one), we consider a point $P=(\hat{x},\hat{t})$ inside the wave and a characteristic curve joining the origin $(0,0)$ and P. The speed of the characteristic is:

$$u-\sqrt{gd+\frac{A(d^2)}{3\gamma}+\frac{2}{3}Ad\psi}=\frac{dx}{dt}=\frac{\hat{x}}{\hat{t}}. \tag{6.1}$$

We can also connect P to the left data state via the generalized Riemann invariant; Eq. (3.8) gives:

$$u_{*L}=u_L-f_R(d_{*L},d_L). \tag{6.2}$$

The simultaneous solution (through Newton procedure) of Eqs. (6.1) and (6.2) for u and d gives the required solution. The solution in the right rarefaction fan or in the rarefaction fan of a compound wave can be found with an analogous procedure.

7 Dry-bed conditions

In this section we give the analytical solution of the Riemann problem for the cases in which dry regions are either present at the initial time or appear as a consequence of the interaction of the two left and right wet-bed states. In the former situation the initial condition is given by a wet region adjacent to a dry region, while in the latter one the whole domain is initially wet. Since in a zero-depth region any equation based on the continuum assumption is not applicable, the solution of the Riemann problem has to be found in the wet region up to the boundary between wet and dry regions, the boundary being part of the solution itself.

First of all, it is possible to demonstrate that a shock wave cannot be adjacent to a dry-bed region. Consider the Riemann problem (2.1) such that $\mathbf{U}_L$ is the data for a wet-bed portion ($d_L>0$) and $\mathbf{U}_R$ is the data for the dry-bed region ($d_R=0$). As the dry-bed region is on the right, the wave family λ_1 is absent, no medium for its propagation being available. Suppose that $\mathbf{U}_L$ and $\mathbf{U}_R$ are connected by a 1-shock wave of speed S. Application of the Rankine-Hugoniot conditions gives $S=u_L$, but this result clearly contradicts the entropy condition necessary to have a shock wave:

$$\lambda_1(\mathbf{U}_L)>S \quad\Longleftrightarrow\quad u_L-\sqrt{gd_L+\frac{Ad_L^2}{3\gamma}+\frac{2}{3}Ad_L\psi_L}>S=u_L, \tag{7.1}$$

demonstrating the above statement.

There are three possible cases to be considered: one first case in which the dry-bed is on the right-hand side, one second case in which the dry-bed on the left-hand side and one last case in which a dry-bed is not present at $t=0$, but it is generated because of the interaction of the data states $\mathbf{U}_L$ and $\mathbf{U}_R$. If the dry-bed is on the left side, the wave patterns and the solution strategy are symmetrical to those shown for the case of right dry-bed.

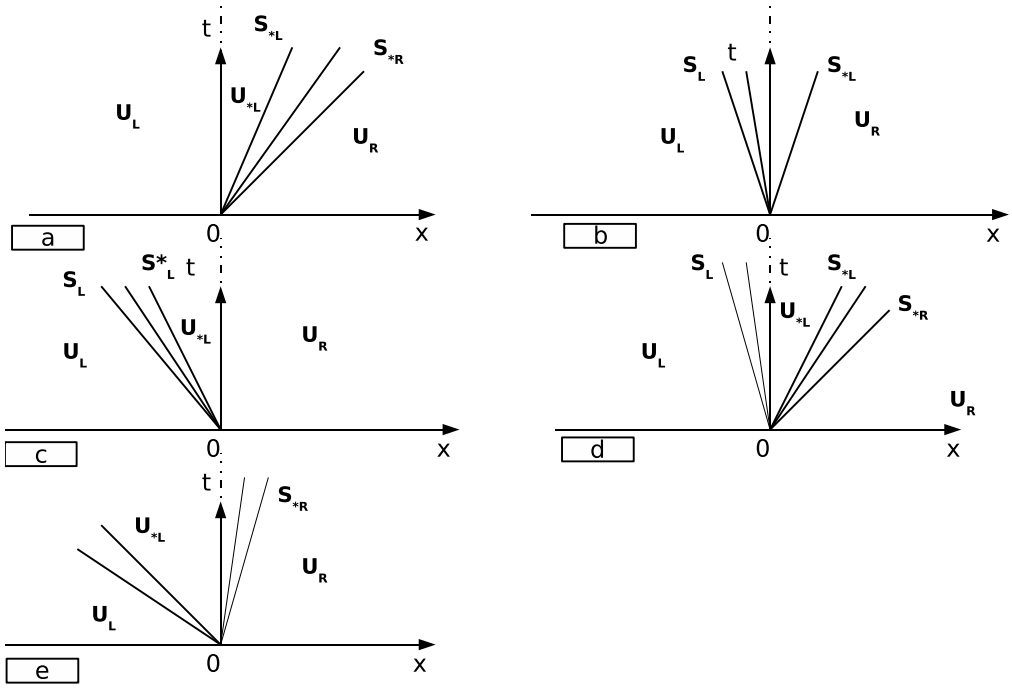

Figure 14: Possible wave patterns if the dry-bed is on the right side.

7.1 The dry-bed is on the right side

If the initial condition presents a dry-bed region on the right side, four possible configurations of the solution can be developed (see Fig. 14). Notice that in all the cases the 4-wave is absent, as there is no water for it to propagate through, while the contact discontinuities associated to the eigenvalues λ_2 and λ_3 can be either present or not depending on the position of the dry-wet interface.

7.1.1 Configuration a

In this case the rarefaction associated to λ_1 lies on the right of the t-axis. This configuration takes place if the following conditions are satisfied:

$$\lambda_1(\mathbf{U}_L)>0, \quad \lambda_1(\mathbf{U}_{*L})>0 \quad \text{and} \quad \lambda_1(\mathbf{U}_{*R})=S_{*R}>0, \tag{7.2}$$

where S_{*R} is the slope of the λ_1 characteristic curve at the wet-dry interface (see Fig. 14). The following equation system applies:

$$\begin{cases} d_{*R}=0, \\ d_L u_L = d_{*L} u_{*L}, \\ \dfrac{g d_L^2}{2}+\dfrac{(u_L d_L)^2}{d_L}+\dfrac{A d_L^2}{3}\psi_L = \dfrac{g d_{*L}^2}{2}+\dfrac{(u_{*L} d_{*L})^2}{d_{*L}}+\dfrac{A d_{*L}^2}{3}\psi_{*L}, \\ u_{*R}=u_{*L}-f_R(d_{*L},d_{*R},\psi_{*L}), \end{cases} \tag{7.3}$$

where

$$\psi_{*L} = \psi_R + \frac{d_{*L}}{\gamma}. \tag{7.4}$$

Such a system can be solved by using a standard multivariate Newton method for non-linear systems of equations.

7.1.2 Configuration b

This configuration takes place if $K_L = K_R$. In this case the solution pattern of the DNSWE reduces to the classical NSWE one and the system to be solved becomes:

$$\begin{cases} d_{*L} = 0, \\ u_{*L} = u_L - f_R(d_{*L}, d_L, \psi_L), \end{cases} \tag{7.5}$$

with

$$\psi_{*L} = \psi_L - \frac{d_L}{\gamma}. \tag{7.6}$$

7.1.3 Configuration c

In this configuration, which occurs if

$$\lambda_1(\mathbf{U}_L) < 0, \quad \lambda_1(\mathbf{U}_{*L}) < 0 \quad \text{and} \quad \lambda_1(\mathbf{U}_{*R}) < 0, \tag{7.7}$$

the contact discontinuities do not exist, as the t-axis lies in a dry region. The set of equations to be solved is the same of 'Configuration b'.

7.1.4 Configuration d

In this configuration the eigenvalue λ_1 changes its sign and interacts with the 0-wave giving rise to a resonance phenomenon. A compound wave appears in the solution pattern. The condition for this configuration to occur are:

$$\lambda_1(\mathbf{U}_L) < 0, \quad \lambda_1(\mathbf{U}_{*L}) > 0, \quad \lambda_1(\mathbf{U}_{*R}) = S_{*R} > 0 \quad \text{and} \quad K_L > K_R, \tag{7.8}$$

To solve this configuration it is possible to use the same strategy used in 'Configuration d' for the wet-bed case. Once identified a point B very close to the t-axis, but on the left side of it, the system of equations to be solved is the following:

$$\begin{cases} d_{*R} = 0, \\ u_B = u_L - f_R(d_B, d_L, \psi_B), \\ d_B u_B = d_{*L} u_{*L}, \\ \dfrac{g d_B^2}{2} + \dfrac{(u_B d_B)^2}{d_B} + \dfrac{A d_B^2}{3}\psi_B = \dfrac{g d_{*L}^2}{2} + \dfrac{(u_{*L} d_{*L})^2}{d_{*L}} + \dfrac{A d_{*L}^2}{3}\psi_{*L}, \\ u_{*R} = u_{*L} + f_R(d_{*L}, d_{*R}, \psi_{*L}), \end{cases} \tag{7.9}$$

where

$$\psi_B = \psi_L + \frac{d_B - d_L}{\gamma} \quad \text{and} \quad \psi_{*L} = \psi_R + \frac{d_{*R}}{\gamma}. \tag{7.10}$$

7.1.5 Configuration e

This configuration also presents a compound wave due to the interaction of the 1-wave with the contact discontinuity because of the presence of a state at which $\lambda_1 = 0$. This configuration occurs if the following conditions are verified:

$$\lambda_1(\mathbf{U}_{*L}) < 0, \quad \lambda_1(\mathbf{U}_{*R}) = S_{*R} > 0 \quad \text{and} \quad K_R > K_L, \tag{7.11}$$

Solution is achieved by the same strategy used in 'Configuration e' for the wet bed case. Once identified a point B very close to the t-axis, but on the right side of it, the system of equations to be solved is the following:

$$\begin{cases} d_{*R} = 0, \\ u_{*L} = u_L - f_{R,S}(d_B, d_L, \psi_L), \\ d_B u_B = d_{*L} u_{*L}, \\ \dfrac{g d_B^2}{2} + \dfrac{(u_B d_B)^2}{d_B} + \dfrac{A d_B^2}{3}\psi_B = \dfrac{g d_{*L}^2}{2} + \dfrac{(u_{*L} d_{*L})^2}{d_{*L}} + \dfrac{A d_{*L}^2}{3}\psi_{*L}, \\ u_{*R} = u_B + f_R(d_{*L}, d_B, \psi_B), \end{cases} \tag{7.12}$$

where

$$\psi_B = \psi_L + \frac{d_B}{\gamma}. \tag{7.13}$$

7.2 The dry bed is generated in the middle

For general wet-bed initial conditions, there can be special combinations of left and right variables which can produce the generation of dry-bed in the middle of the domain. Unfortunately, it is not possible to find a priori a condition on $\mathbf{U}_L$ and $\mathbf{U}_R$ which can identify such a configuration of the solution, as is the case of shallow water equations (see [15]). However, as the DNSWE always require a set of trial values to start the solution procedure, the generation of dry-bed in the middle can be identified by using them. In this case, the only possible wave pattern is the one shown in Fig. 15. The system of equations to be solved is the following:

$$\begin{cases} d_{*L} = 0, \\ d_{*R} = 0, \\ u_{*L} = u_L - f_R(d_{*L}, d_L, \psi_L), \\ u_{*R} = u_R - f_R(d_{*R}, d_R, \psi_R). \end{cases} \tag{7.14}$$

8 Test cases

In this section we present some analytical solutions of the Riemann problem for the homogeneous DNSWE. Such solutions are compared with numerical solutions obtained

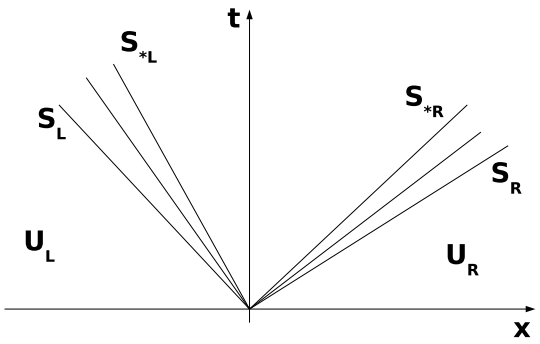

Figure 15: The dry-bed is generated in the middle.

by using both a Rusanov and a FORCE flux in the frame of the second-order MUSCL-Hancock Method (see [17]). The test case initial conditions are shown in Table 2 (L is the length of the computational domain). Notice that the output times are different for all the test cases: in fact, as the wave celerity depends on the initial conditions, we have to choose appropriate output times in order to see all the waves within the computational domain.

Table 2: Test case initial conditions for DNSWE, over both Shallow Water (SW), Intermediate Depth (ID) and Dry Bed (DB) conditions.

test	d_L	u_L	ψ_L	ϕ_L	d_R	u_R	ψ_R	ϕ_R	L	x_{gate}	Conf.	Cond.
1	0.01	-0.005	5.0	0.0	0.01	0.005	5.0	0.0	1.0	0.5	a	SW
2	1.0	0.0	10.0	1.0	0.5	0.0	20.0	5.0	6.0	3.0	a	ID
3	1.0	10.0	-10.0	5.0	0.5	0.0	10.0	1.0	6.0	3.0	b	ID
4	1.0	0.0	50.0	5.0	0.5	0.0	-10.0	1.0	6.0	3.0	d	ID
5	0.1	0.0	20.0	5.0	1.0	-2.5	-10.0	1.0	6.0	3.0	e	ID
6	0.5	0.5	20.0	5.0	0.0	0.0	0.0	0.0	6.0	3.0	d dry	DB
7	0.5	-8.0	20.0	5.0	0.5	8.0	10.0	0.0	6.0	3.0	mid-dry	DB

The test case conditions are both of shallow and intermediate water depths. In particular, shallow water conditions can be identified by exploiting the fact that, over very small depths, the first two eigenvalues of the DNSWE tend to the eigenvalues of the classical nonlinear shallow water equations. This happens when:

$$\frac{A}{3g}\left|\frac{d}{\gamma}+2\psi\right| \ll 1. \tag{8.1}$$

Since $A=1s^{-1}$, $3g/A \simeq 29.43$ and, consequently, a good approximation of (8.1) is:

$$\left|\frac{d}{\gamma}+2\psi\right| \leq 1\text{m}. \tag{8.2}$$

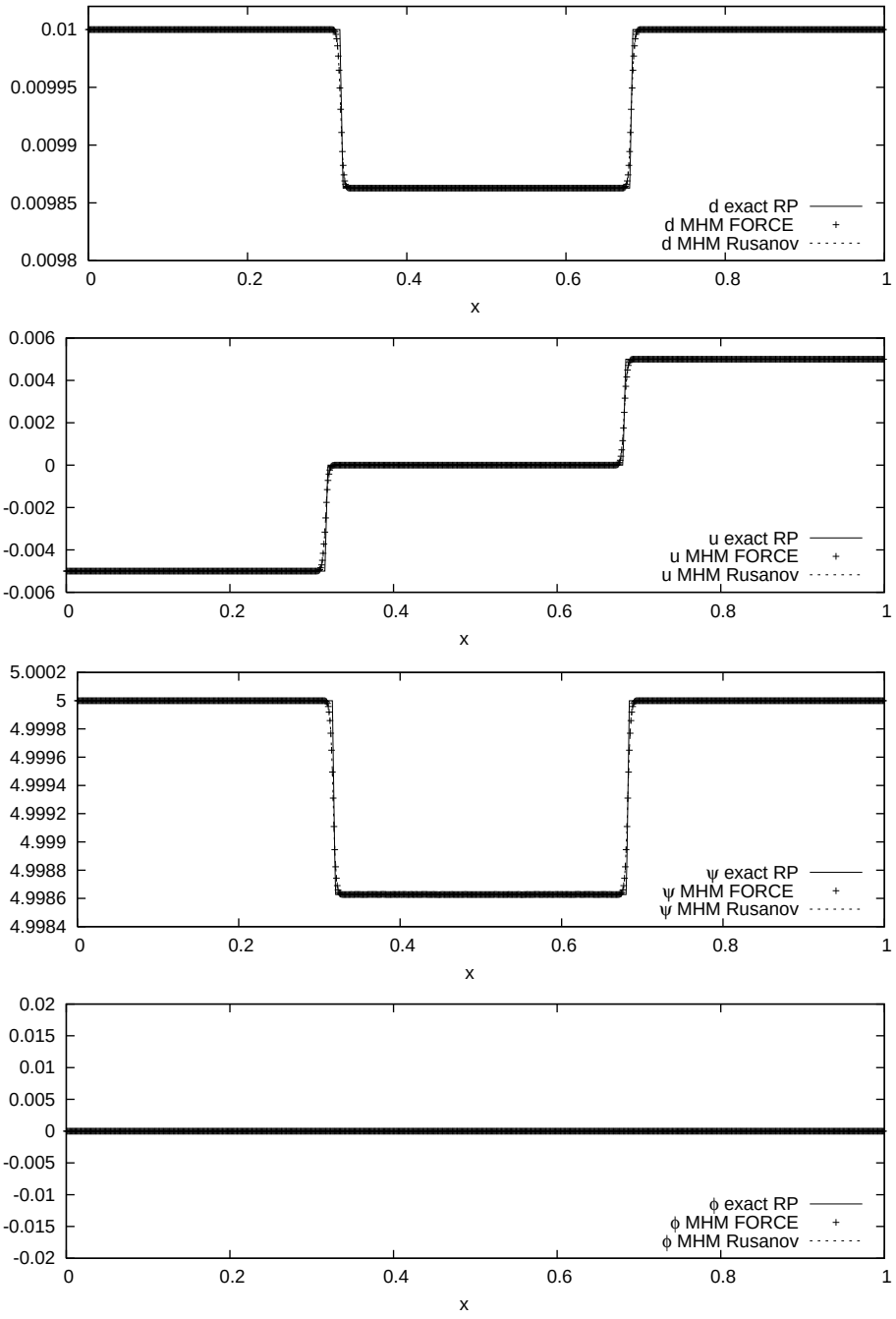

Figure 16: Test 1. Numerical solution for ψ and ϕ obtained using the MUSCL-Hancock method with both Rusanov flux (dashed line) and FORCE flux (crosses) and the exact solution (line) of the Riemann problem for the DNSWE, at $t=0.5s$ (configuration a of Fig. 12).

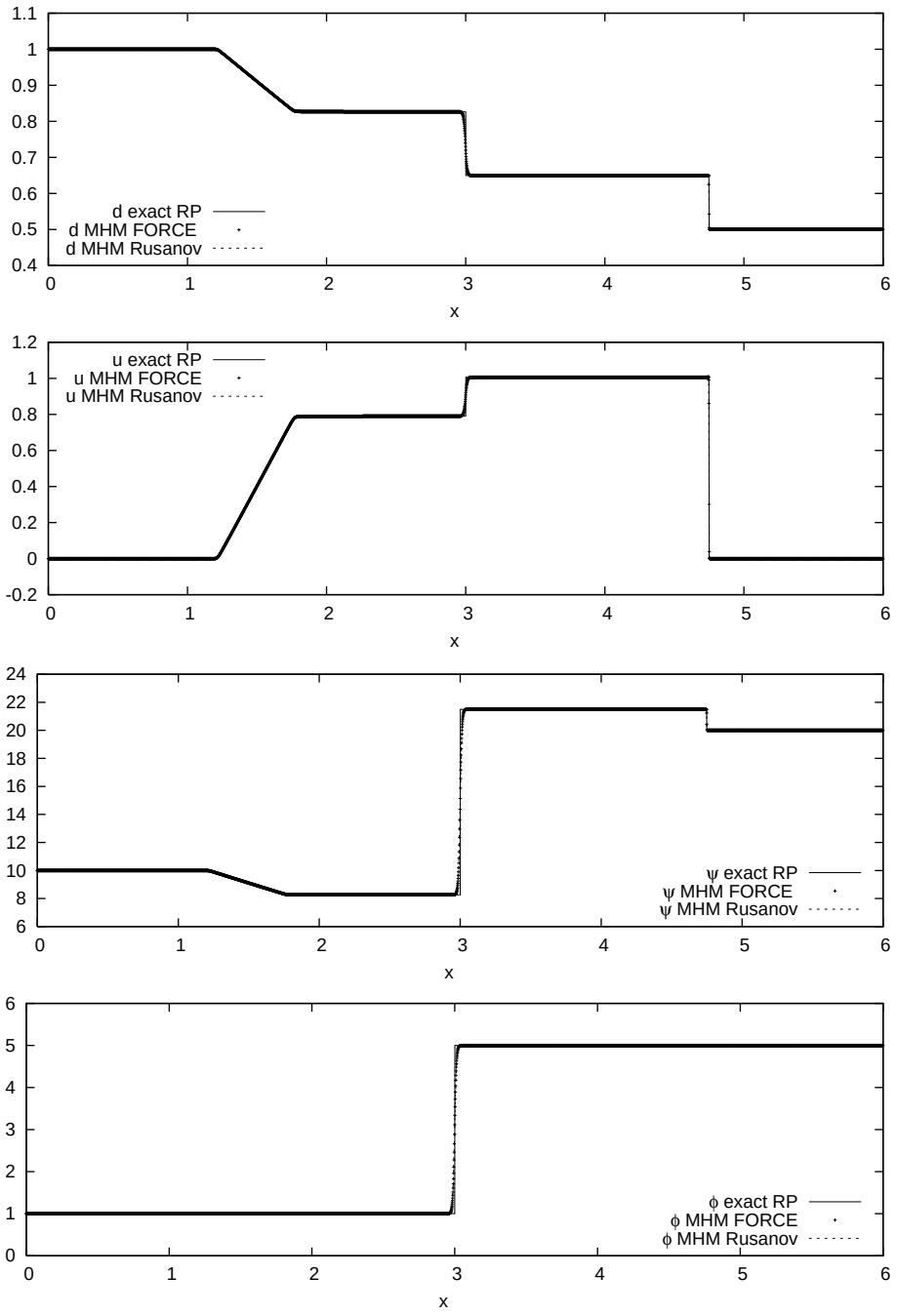

Figure 17: Test 2. Numerical solution for ψ and ϕ obtained using the MUSCL-Hancock method with both Rusanov flux (dashed line) and FORCE flux (crosses) and the exact solution (line) of the Riemann problem for the DNSWE, at $t=0.4s$ (configuration a of Fig. 12).

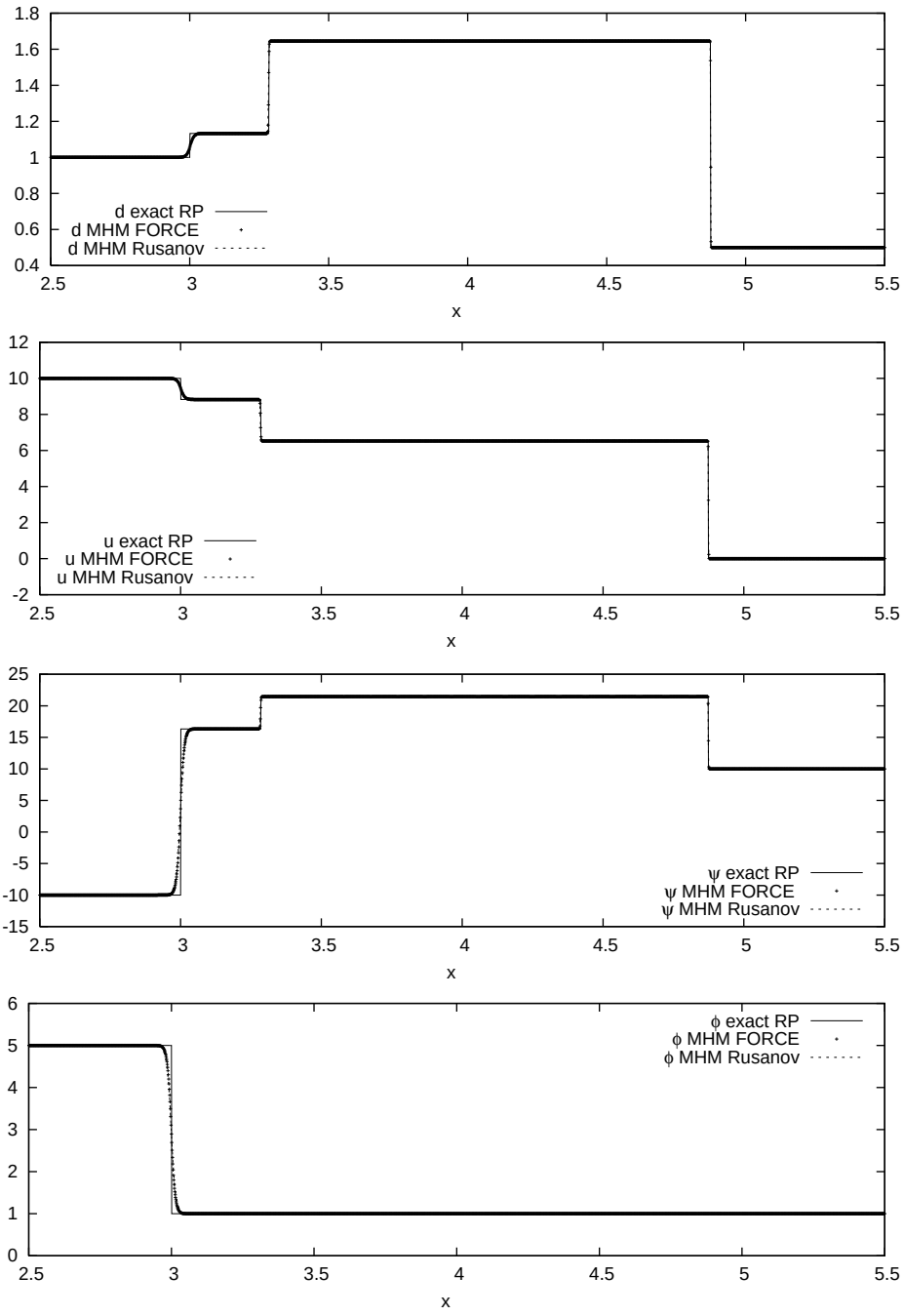

Figure 18: Test 3. Numerical solution for ψ and ϕ obtained using the MUSCL-Hancock method with both Rusanov flux (dashed line) and FORCE flux (crosses) and the exact solution (line) of the Riemann problem for the DNSWE, at $t=0.2s$ (configuration b of Fig. 12).

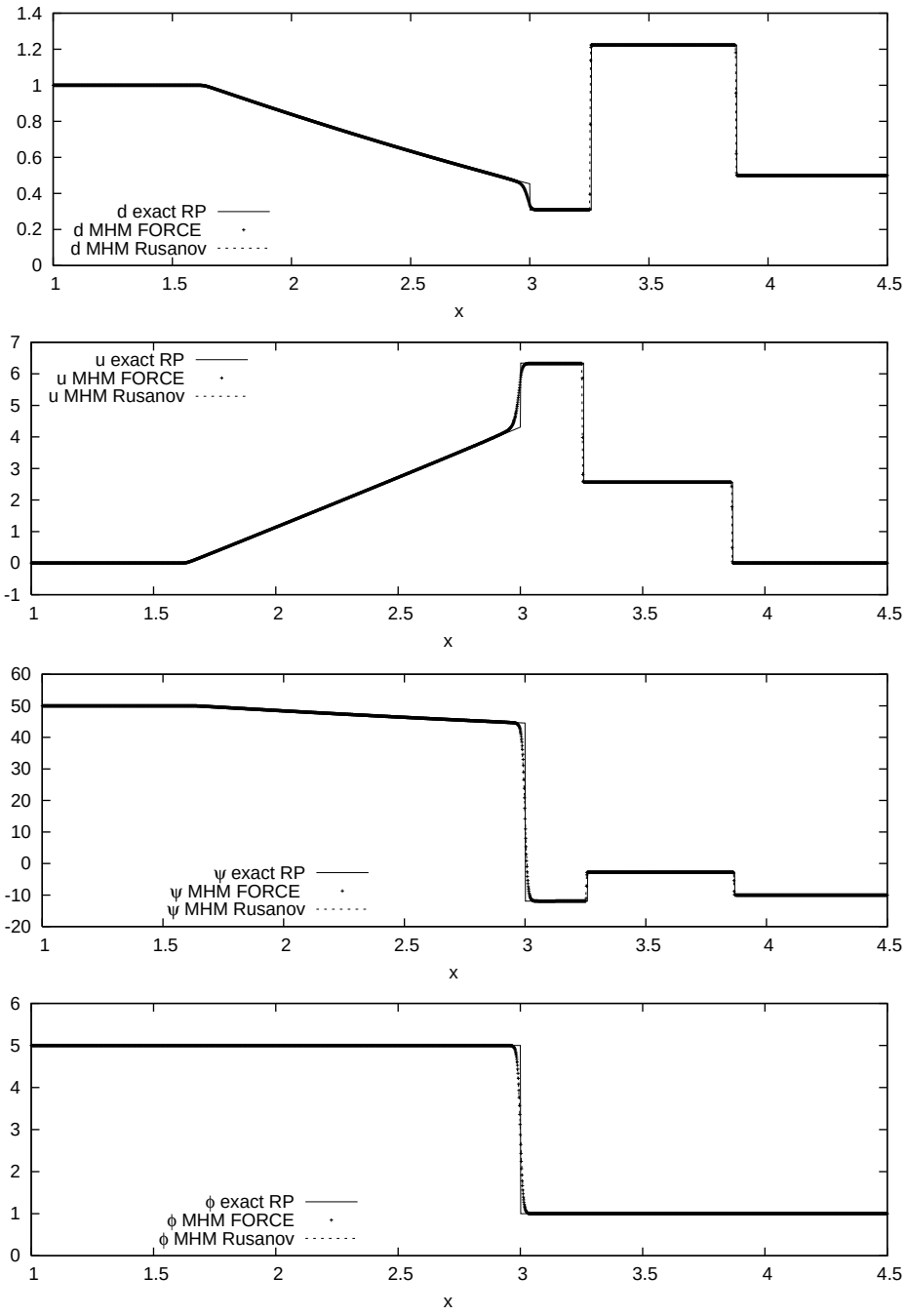

Figure 19: Test 4. Numerical solution for ψ and ϕ obtained using the MUSCL-Hancock method with both Rusanov flux (dashed line) and FORCE flux (crosses) and the exact solution (line) of the Riemann problem for the DNSWE, at $t=0.2s$ (configuration d of Fig. 12).

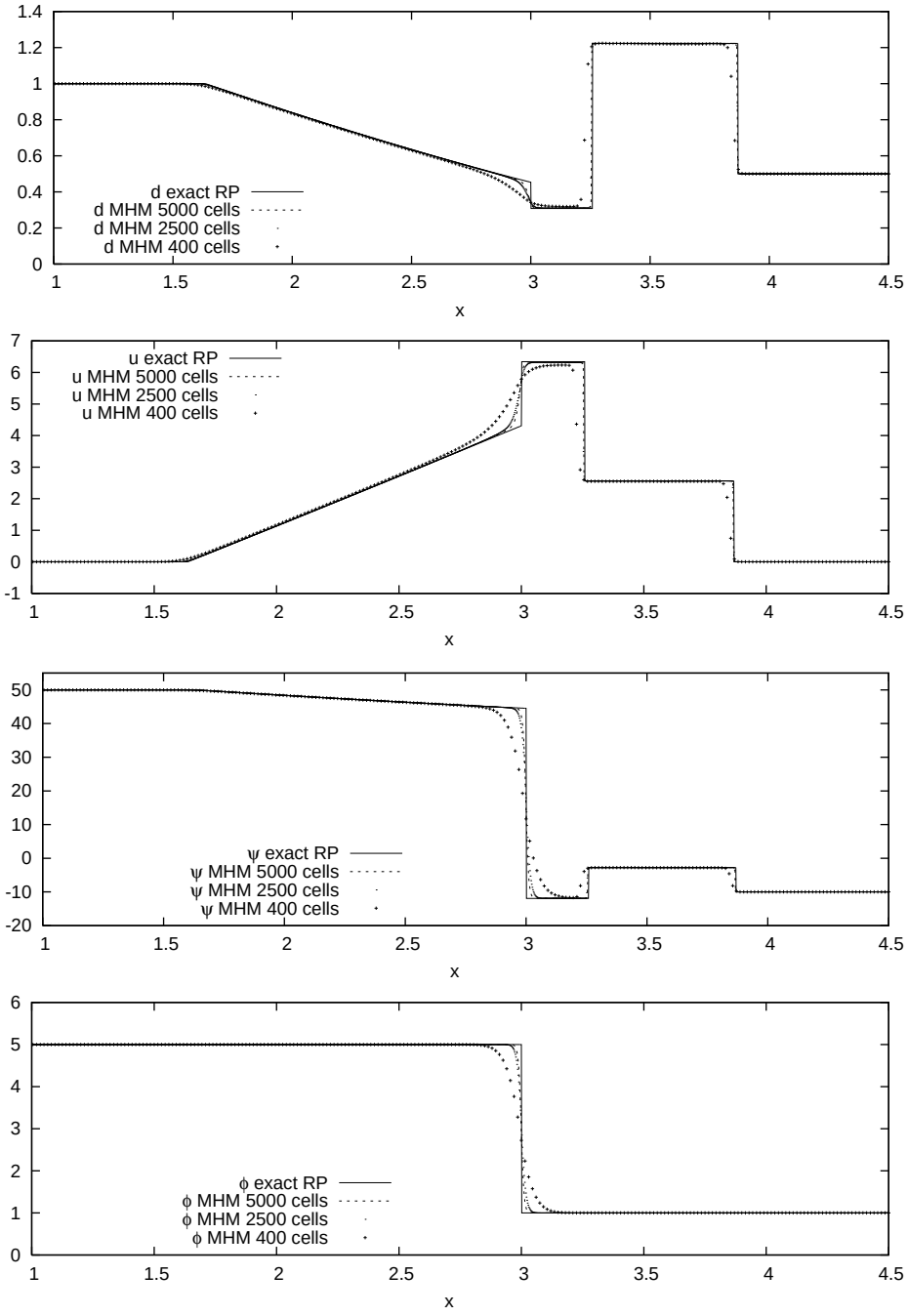

Figure 20: Test 4. Convergence test for the numerical solution for ψ and ϕ obtained using the MUSCL-Hancock method (FORCE flux) over a mesh of 400 (crosses), 2500 (dots) and 5000 cells (dashed line). The thick line represents the analytical solution at $t=0.2s$.

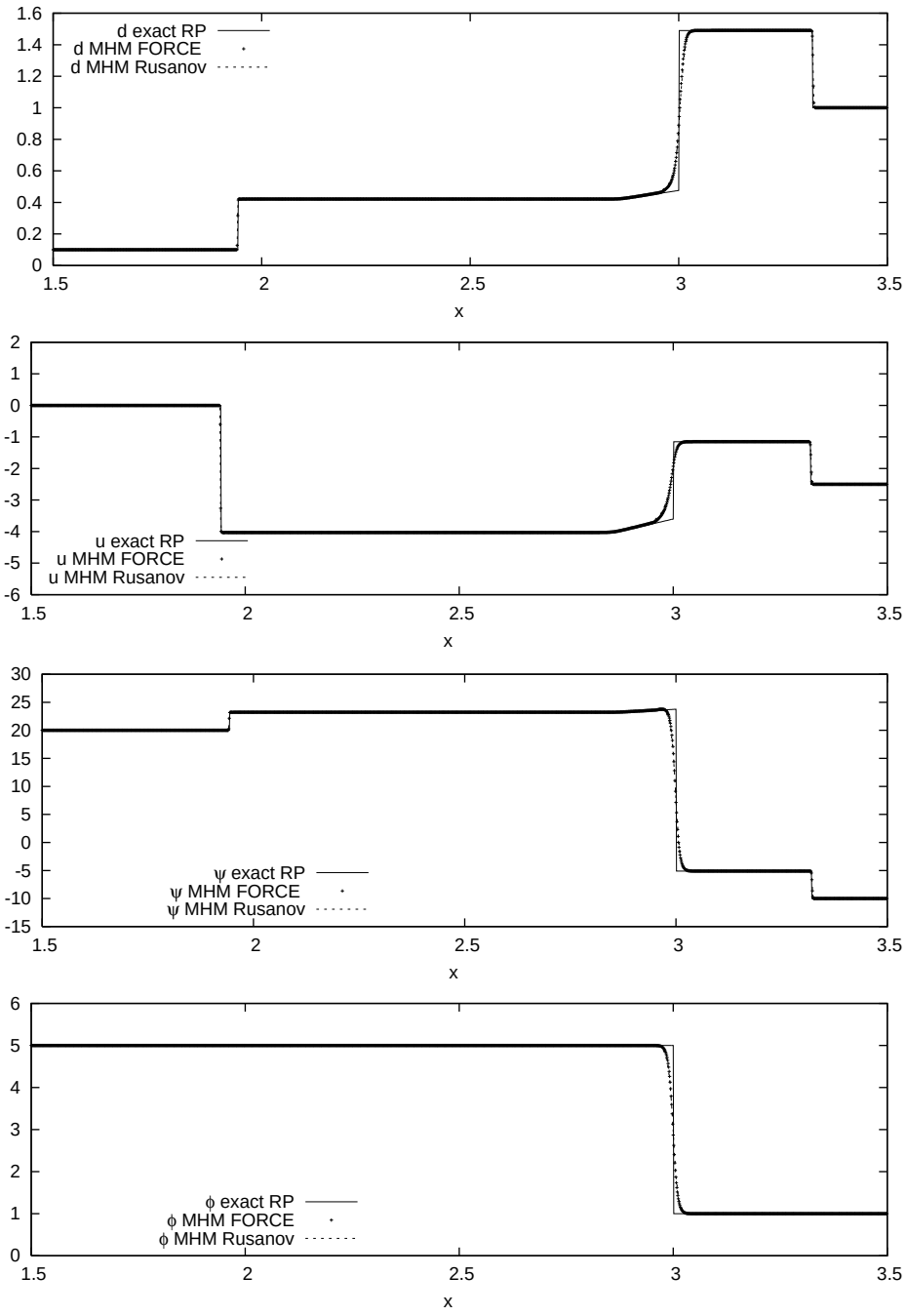

Figure 21: Test 5. Numerical solution for ψ and ϕ obtained using the MUSCL-Hancock method with both Rusanov flux (dashed line) and FORCE flux (crosses) and the exact solution (line) of the Riemann problem for the DNSWE, at $t=0.2s$ (configuration e of Fig. 12).

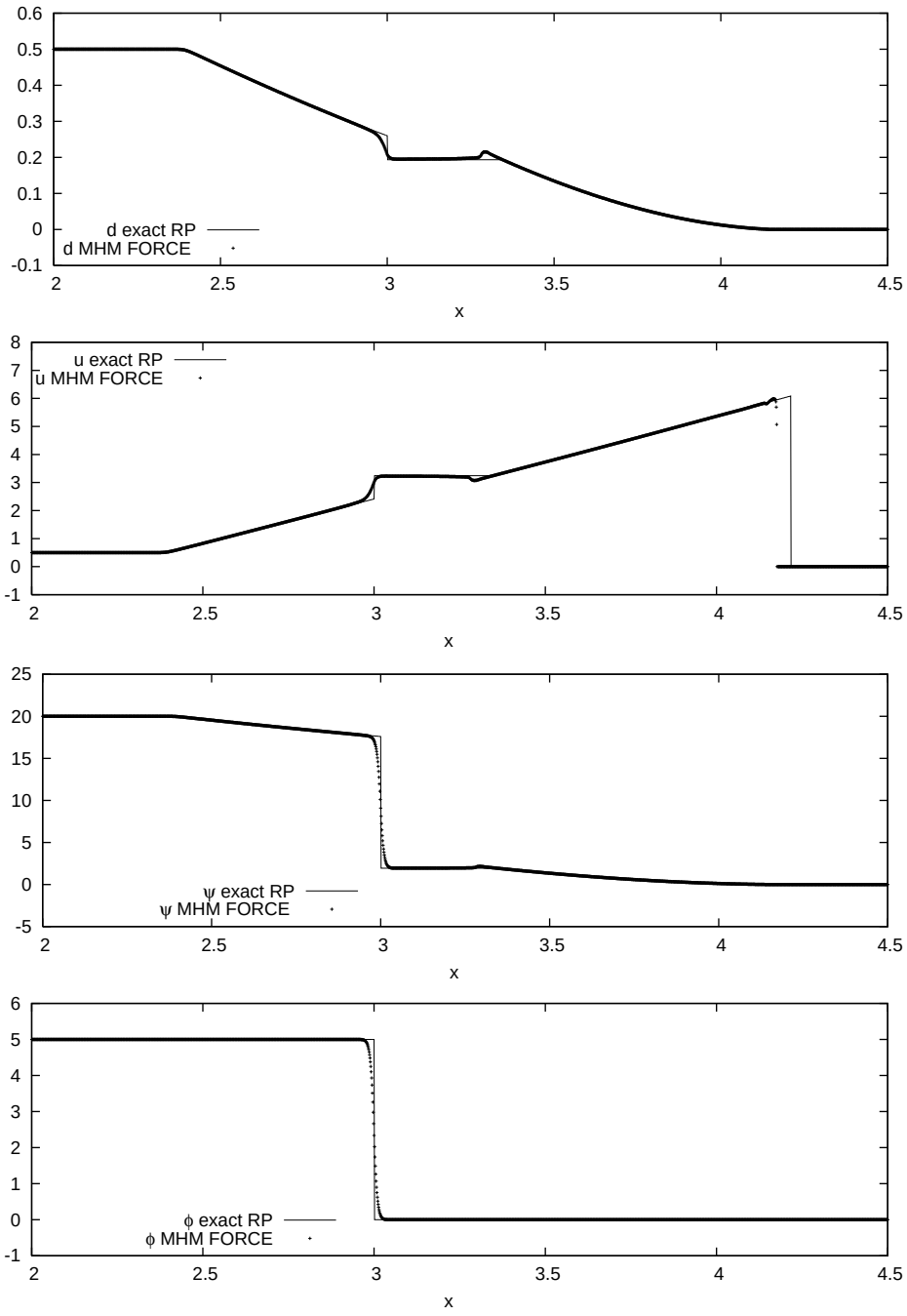

Figure 22: Test 6. Numerical solution for ψ and ϕ obtained using the MUSCL-Hancock method with a FORCE flux (crosses) and the exact solution (line) of the Riemann problem for the DNSWE, at $t=0.2s$ (configuration d dry of Fig. 14).

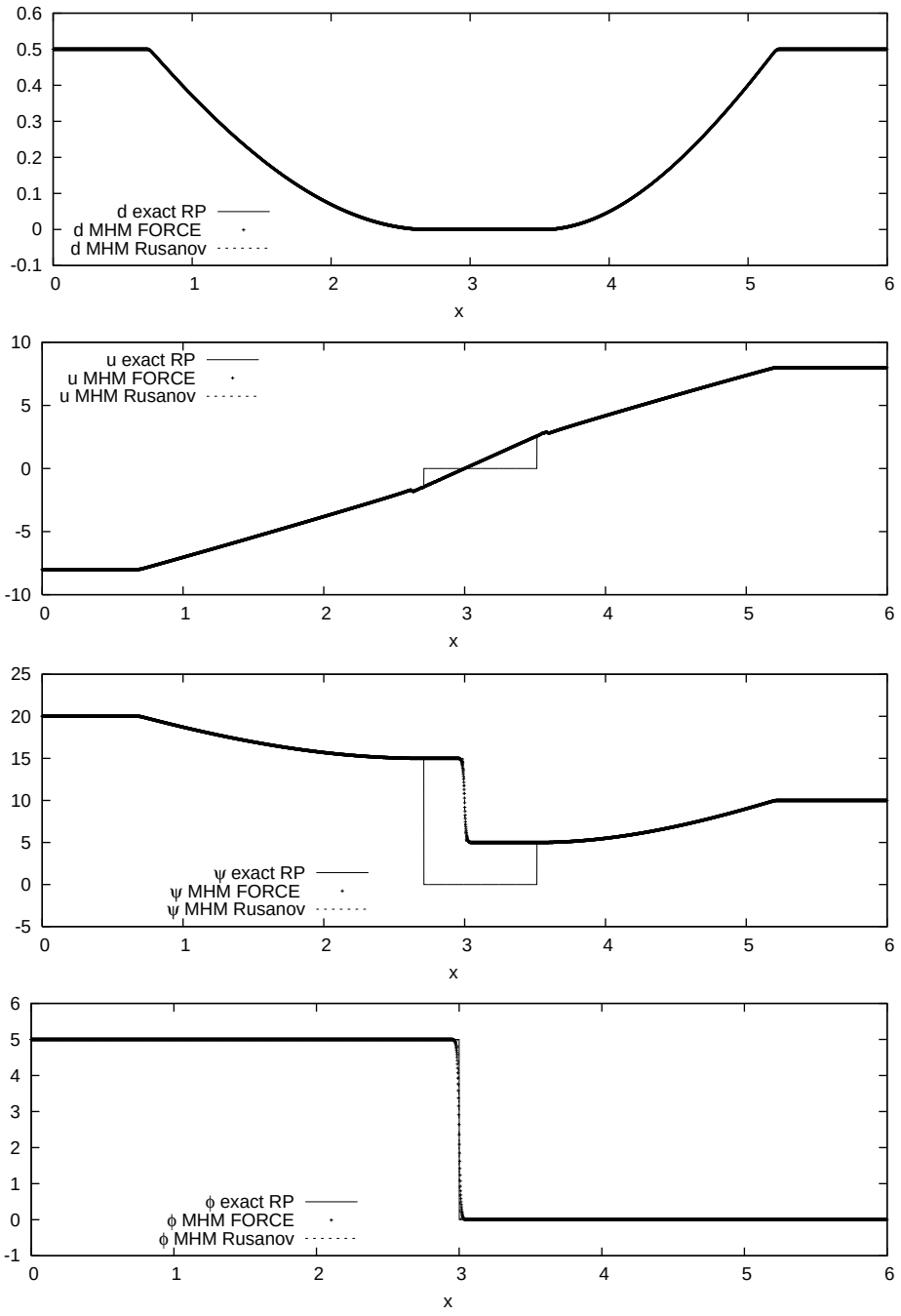

Figure 23: Test 7. Numerical solution for ψ and ϕ obtained using the MUSCL-Hancock method with both Rusanov flux (dashed line) and FORCE flux (crosses) and the exact solution (line) of the Riemann problem for the DNSWE, at $t=0.2s$ (configuration of dry bed in the middle of Fig. 15).

We also investigate the behaviour of the solution for some relevant cases of resonance and for dry-bed conditions. In all the test cases, $N_{cells}=5000$, $\gamma=0.1$ and $C_{cfl}=0.9$ (except for Test 1, in which $N_{cells}=1000$, the computational domain being shorter than the others). A convergence test is also shown, in which the numerical solution is obtained over meshes of 400, 2500, and 5000 cells (test conditions are those of Test 4).

All the test cases show a very good agreement between the numerical and the analytical solutions of the Riemann problem, over both shallow and intermediate water depths. In particular, the numerical solutions constitute a cross-check of the analytical solution, as in the case of discontinuous solutions, since the numerical method chooses the entropy-satisfying solution by default, as a result of its numerical viscosity. It is reassuring that the correct wave pattern of the solution, the correct values of the variables in the constant regions $\mathbf{U}_{*L}$ and $\mathbf{U}_{*R}$ and correct sampling of the solution have been attained. This is true also in complex cases, like those containing compound waves. Notice that the only differences between the numerical and the analytical solution can be seen in Tests 6 and 7 (Figs. 22 and 23). Such differences are due to the fact that the numerical solvers fail when facing dry-bed conditions.

9 Conclusions

Compared to the classical Nonlinear Shallow Water Equations and to the many available Boussinesq models, the Dispersive Nonlinear Shallow Water Equations (DNSWE), proposed by Antuono, Liapideskii and Brocchini [1], show many advantages. In particular they are able not only to simply treat wave-breaking and the shoreline motion, because of their hyperbolic character, but they also allow to model dispersive effects.

Since the DNSWE are a set of hyperbolic equations with stiff source terms, they require appropriate numerical solution techniques. Very commonly used approaches to solve system of balance laws with stiff source terms are splitting schemes. These schemes consist in solving iteratively the associated system of conservation laws with a classical finite volume scheme and the associated system of ordinary derivative equations with an appropriate numerical tool. In particular, powerful numerical fluxes to solve hyperbolic systems of conservation laws are based on the solution of the Riemann problem for the system of conservation laws.

In the present work an analytical solution of the Riemann problem for the homogeneous part of the DNSWE is proposed, over both wet and dry bed conditions. All the possible wave patterns of the solution are deeply analyzed and a particular care is devoted to those cases in which one of the eigenvalues of the system becomes zero. Such configurations can allow for the formation of compound waves, which need appropriate equations to be recognized and solved. The validity of the presented analytical solution is confirmed by comparisons with accurate numerical solutions, obtained by using dissipative methods that do not make explicit use of the solution of the local Riemann problem. A very good agreement between the analytical solution and numerical ones is shown in

all the Riemann problem test cases presented.

Thanks to the good results obtained, the proposed analytical Riemann solver could be used for the construction of a Godunov-type solver for the homogeneous DNSWE, to be coupled with appropriate numerical tools for the associated system of ordinary derivative equations, in order to get a consistent, stable and accurate scheme for the complete DNSWE. Such a complete solver, which is the goal of current undergoing studies, would allow to correctly model nearshore hydrodynamics and could be applied to study different physical phenomena of wave propagation over both intermediate and shallow water depths.

Acknowledgments

The authors acknowledge the partial financial support received by the E.U. through the INTAS Project 06-1000013-9236 and by the "Ministero Infrastrutture e Trasporti" within the "Programma di Ricerca 2007-2009". Acknowledgments are also due to Prof. Maurizio Brocchini for his useful comments and suggestions.

References

[1] M. Antuono, V. Liapidevskii and M. Brocchini, Dispersive nonlinear shallow water equations, Stud. Appl. Maths., 122 (2009), 1-28.
[2] W. Bao and S. Jin, Error estimates on the random projection methods for hyperbolic conservation laws with stiff reaction terms, Appl. Numer. Math., 43 (2002), 315-333.
[3] G. Bellotti and M. Brocchini, On the shoreline boundary conditions for Boussinesq-type models, Int. J. Numer. Meth. Fluids, 37(4) (2001), 479-500.
[4] B. Engquist and S. Osher, One sided difference approximations for nonlinear conservation laws, Math. Comput., 36 (1981), 321-351.
[5] E. Burman and L. Sainsaulieu, Numerical analysis of two operator splitting methods for an hyperbolic system of conservation laws with stiff relaxation, Comput. Method. Appl. Mech. Engrg., 128 (1995), 291-314.
[6] R. E. Caflish, S. Jin and G. Russo, Uniformly accurate schemes for hyperbolic systems with relaxation, SIAM J. Numer. Anal., 34 (1997), 246-281.
[7] S. K. Godunov, Finite difference methods for the computation of discontinuous solutions of the equations of fluid dynamics, Mathematics of the USSR, Sbornik, 47 (1959), 271-306.
[8] A. Jeffrey, Quasilinear Hyperbolic Systems and Waves, Pitman, 1976.
[9] E. Isaacson and B. Temple, Nonlinear resonance in systems of conservation laws, J. Appl. Math., 52 (1992), 1260-1278.
[10] F. Miniati and P. Colella, A modified higher order Godunov's scheme for stiff source conservative hydrodynamics, J. Comput. Phys., 224(2) (2007), 519-538.
[11] S. Osher and F. Solomon, Upwind difference schemes for hyperbolic conservation laws, Math. Comput., 38 (1982), 339-374.
[12] D. H. Peregrine, Long waves on a beach, J. Fluid Mech., 27 (1967), 815-827.
[13] W. H. Press, S. A. Teukolsky, W. T. Vetterling and B. P. Flannery, Numerical Recipes in Fortran 77, vol. 1, Cambridge University Press, 1996.

[14] P. L. Roe, Approximate Riemann solvers, parameter vectors, and dfference schemes, J. Comput. Phys., 43 (1981), 357-372.
[15] E. F. Toro, Shock Capturing Methods for Free-Surface Shallow Flows, John Wiley and Sons, 2001.
[16] E. F. Toro, Riemann Solvers and Numerical Methods for Fluid Dynamics, 2nd ed., Springer, 1999.
[17] B. van Leer, On the relation between the upwind-differencing schemes of Godunov, Enguist-Osher and Roe, SIAM J. Sci. Stat. Comput., 5(1) (1985), 1-20.